

CERN-PH-EP-2012-191

Submitted to: EPJC

Jet energy resolution in proton-proton collisions at $\sqrt{s} = 7$ TeV recorded in 2010 with the ATLAS detector

The ATLAS Collaboration

Abstract

The measurement of the jet energy resolution is presented using data recorded with the ATLAS detector in proton-proton collisions at $\sqrt{s} = 7$ TeV. The sample corresponds to an integrated luminosity of 35 pb^{-1} . Jets are reconstructed from energy deposits measured by the calorimeters and calibrated using different jet calibration schemes. The jet energy resolution is measured with two different in situ methods which are found to be in agreement within uncertainties. The total uncertainties on these measurements range from 20% to 10% for jets within $|y| < 2.8$ and with transverse momenta increasing from 30 GeV to 500 GeV. Overall, the Monte Carlo simulation of the jet energy resolution agrees with the data within 10%.

Jet energy resolution in proton-proton collisions at $\sqrt{s} = 7$ TeV recorded in 2010 with the ATLAS detector

The ATLAS Collaboration

Address(es) of author(s) should be given

Received: date / Revised version: date

Abstract. The measurement of the jet energy resolution is presented using data recorded with the ATLAS detector in proton-proton collisions at $\sqrt{s} = 7$ TeV. The sample corresponds to an integrated luminosity of 35 pb^{-1} . Jets are reconstructed from energy deposits measured by the calorimeters and calibrated using different jet calibration schemes. The jet energy resolution is measured with two different in situ methods which are found to be in agreement within uncertainties. The total uncertainties on these measurements range from 20% to 10% for jets within $|y| < 2.8$ and with transverse momenta increasing from 30 GeV to 500 GeV. Overall, the Monte Carlo simulation of the jet energy resolution agrees with the data within 10%.

PACS. XX.XX.XX No PACS code given

Contents

| | | | | | |
|------|--|----|----|---|----|
| 1 | Introduction | 2 | 12 | Improvement in jet energy resolution using tracks | 13 |
| 2 | The ATLAS detector | 2 | 13 | Summary | 13 |
| 3 | Monte Carlo simulation | 2 | 14 | Acknowledgements | 13 |
| 3.1 | Event generators | 2 | | | |
| 3.2 | Simulation of the ATLAS detector | 3 | | | |
| 3.3 | Simulated pile-up samples | 3 | | | |
| 4 | Event and jet selection | 3 | | | |
| 5 | Jet energy calibration | 4 | | | |
| 5.1 | The EM+JES calibration | 4 | | | |
| 5.2 | The Local Cluster Weighting (LCW) calibration | 4 | | | |
| 5.3 | The Global Cell Weighting (GCW) calibration | 4 | | | |
| 5.4 | The Global Sequential (GS) calibration | 4 | | | |
| 5.5 | Track-based correction to the jet calibration | 4 | | | |
| 6 | In situ jet resolution measurement using the dijet balance method | 5 | | | |
| 6.1 | Measurement of resolution from asymmetry | 5 | | | |
| 6.2 | Soft radiation correction | 5 | | | |
| 6.3 | Particle balance correction | 6 | | | |
| 7 | In situ jet resolution measurement using the bisector method | 7 | | | |
| 7.1 | Bisector rationale | 7 | | | |
| 7.2 | Validation of the soft radiation isotropy with data | 7 | | | |
| 8 | Performance for the EM+JES calibration | 7 | | | |
| 9 | Closure test using Monte Carlo simulation | 9 | | | |
| 10 | Jet energy resolution uncertainties | 9 | | | |
| 10.1 | Experimental uncertainties | 9 | | | |
| 10.2 | Uncertainties due to the event modelling in the Monte Carlo generators | 10 | | | |
| 10.3 | Uncertainties on the measured resolutions | 10 | | | |
| 11 | Jet energy resolution for other calibration schemes | 11 | | | |

1 Introduction

Precise knowledge of the jet energy resolution is of key importance for the measurement of the cross-sections of inclusive jets, dijets, multijets or vector bosons accompanied by jets [1–4], top-quark cross-sections and mass measurements [5], and searches involving resonances decaying to jets [6, 7]. The jet energy resolution also has a direct impact on the determination of the missing transverse energy, which plays an important role in many searches for new physics with jets in the final state [8, 9]. This article presents the determination with the ATLAS detector [10, 11] of the jet energy resolution in proton-proton collisions at a centre-of-mass energy of $\sqrt{s} = 7$ TeV. The data sample was collected during 2010 and corresponds to 35 pb^{-1} of integrated luminosity delivered by the Large Hadron Collider (LHC) [12] at CERN.

The jet energy resolution is determined by exploiting the transverse momentum balance in events containing jets with large transverse momenta (p_T). This article is structured as follows: Section 2 describes the ATLAS detector. Sections 3, 4 and 5 respectively introduce the Monte Carlo simulation, the event and jet selection criteria, and the jet calibration methods. The two techniques to estimate the jet energy resolution from calorimeter observables, the *dijet balance method* [13] and the *bisector method* [14], are discussed respectively in Sections 6 and 7. These methods rely on somewhat different assumptions, which can be validated in data and are sensitive to different sources of systematic uncertainty. As such, the use of these two independent in situ measurements of the jet energy resolution is important to validate the Monte Carlo simulation. Section 8 presents the results obtained for data and simulation for the default jet energy calibration scheme implemented in ATLAS. Section 9 compares results of the Monte Carlo simulation in situ methods to the resolutions obtained by comparing the jet energy at calorimeter and particle level. This comparison will be referred to as a closure test. Sources of systematic uncertainty on the jet energy resolution estimated using the available Monte Carlo simulations and collision data are discussed in Section 10. The results for other jet energy calibration schemes are discussed in Sections 11 and 12, and the conclusions can be found in Section 13.

2 The ATLAS detector

The ATLAS detector is a multi-purpose detector designed to observe particles produced in high energy proton-proton collisions. A detailed description can be found in Refs. [10, 11]. The Inner (tracking) Detector has complete azimuthal coverage and spans the pseudorapidity region $|\eta| < 2.5$ ¹. The Inner

¹ The ATLAS reference system is a Cartesian right-handed coordinate system, with the nominal collision point at the origin. The anti-clockwise beam direction defines the positive z -axis, with the x -axis pointing to the centre of the LHC ring. The angle ϕ defines the direction in the plane transverse to the beam (x, y). The pseudorapidity is given by $\eta = -\ln \tan \frac{\theta}{2}$, where the polar angle θ is taken with respect to the positive z direction. The rapidity is defined as $y = 0.5 \times \ln[(E + p_z)/(E - p_z)]$, where E denotes the energy and p_z is the component of the momentum along the z -axis.

Detector consists of layers of silicon pixel, silicon microstrip and transition radiation tracking detectors. These sub-detectors are surrounded by a superconducting solenoid that produces a uniform 2 T axial magnetic field.

The calorimeter system is composed of several sub-detectors. A high-granularity liquid-argon (LAr) electromagnetic sampling calorimeter covers the $|\eta| < 3.2$ range, and it is split into a barrel ($|\eta| < 1.475$) and two end-caps ($1.375 < |\eta| < 3.2$). Lead absorber plates are used over its full coverage. The hadronic calorimetry in the barrel is provided by a sampling calorimeter using steel as the absorber material and scintillating tiles as active material in the range $|\eta| < 1.7$. This tile hadronic calorimeter is separated into a large barrel and two smaller extended barrel cylinders, one on either side of the central barrel. In the end-caps, copper/LAr technology is used for the hadronic end-cap calorimeters (HEC), covering the range $1.5 < |\eta| < 3.2$. The copper-tungsten/LAr forward calorimeters (FCal) provide both electromagnetic and hadronic energy measurements, extending the coverage to $|\eta| = 4.9$.

The trigger system consists of a hardware-based Level 1 (L1) and a two-tier, software-based High Level Trigger (HLT). The L1 jet trigger uses a sliding window algorithm with coarse-granularity calorimeter towers. This is then refined using jets reconstructed from calorimeter cells in the HLT.

3 Monte Carlo simulation

3.1 Event generators

Data are compared to Monte Carlo (MC) simulations of jets with large transverse momentum produced via strong interactions described by Quantum Chromodynamics (QCD) in proton-proton collisions at a centre-of-mass energy of $\sqrt{s} = 7$ TeV. The jet energy resolution is derived from several simulation models in order to study its dependence on the event generator, on the parton showering and hadronisation models, and on tunes of other soft model parameters, such as those of the underlying event. The event generators used for this analysis are described below.

1. PYTHIA 6.4 MC10 tune: The event generator PYTHIA [15] simulates non-diffractive proton-proton collisions using a $2 \rightarrow 2$ matrix element at the leading order (LO) of the strong coupling constant to model the hard sub-process, and uses p_T -ordered parton showers to model additional radiation in the leading-logarithm approximation [16]. Multiple parton interactions [17], as well as fragmentation and hadronization based on the Lund string model [18] are also simulated. The parton distribution function (PDF) set used is the modified leading-order MRST LO* set [19]. The parameters used to describe multiple parton interactions are denoted as the ATLAS MC10 tune [20]. This generator and tune are chosen as the baseline for the jet energy resolution studies.
2. The PYTHIA PERUGIA2010 tune is an independent tune of PYTHIA to hadron collider data with increased final-state radiation to better reproduce the jet and hadronic event shapes observed in LEP and Tevatron data [21]. Parameters sensitive to the production of particles with strangeness and

related to jet fragmentation have also been adjusted. It is the tune favoured by ATLAS jet shape measurements [22].

3. The PYTHIA PARP90 modification is an independent systematic variation of PYTHIA. The variation has been carried out by changing the parameter that controls the energy dependence of the cut-off, deciding whether the events are generated with the matrix element and parton-shower approach, or the soft underlying event [23].
4. PYTHIA8 [24] is based on the event generator PYTHIA and contains several modelling improvements, such as fully interleaved p_T -ordered evolution of multiparton interactions and initial- and final-state radiation, and a richer mix of underlying-event processes. Once fully tested and tuned, it is expected to offer a complete replacement for version 6.4.
5. The HERWIG++ generator [25–28] uses a leading order $2 \rightarrow 2$ matrix element with angular-ordered parton showers in the leading-logarithm approximation. Hadronization is performed in the cluster model [29]. The underlying event and soft inclusive interactions use hard and soft multiple partonic interaction models [30]. The MRST LO* PDFs [19] are used.
6. ALPGEN is a tree-level matrix element generator for hard multi-parton processes ($2 \rightarrow n$) in hadronic collisions [31]. It is interfaced to HERWIG to produce parton showers in leading-logarithm approximation, which are matched to the matrix element partons with the MLM matching scheme [32]. HERWIG is used for hadronization and JIMMY [33] is used to model soft multiple parton interactions. The LO CTEQ6L1 PDFs [34] are used.

3.2 Simulation of the ATLAS detector

Detector simulation is performed with the ATLAS simulation framework [35] based on GEANT4 [36], which includes a detailed description of the geometry and the material of the detector. The set of processes that describe hadronic interactions in the GEANT4 detector simulation are outlined in Refs. [37, 38]. The energy deposited by particles in the active detector material is converted into detector signals to mimic the detector read-out. Finally, the Monte Carlo generated events are processed through the trigger simulation of the experiment and are reconstructed and analysed with the same software that is used for data.

3.3 Simulated pile-up samples

The nominal MC simulation does not include additional proton-proton interactions (pile-up). In order to study its effect on the jet energy resolution, two additional MC samples are used. The first one simulates additional proton-proton interactions in the same bunch crossing (in-time pile-up) while the second sample in addition simulates effects on calorimeter cell energies from close-by bunches (out-of-time pile-up). The average number of interactions per event is 1.7 (1.9) for the in-time (in-time plus out-of-time) pile-up samples, which is a good representation of the 2010 data.

4 Event and jet selection

The status of each sub-detector and trigger, as well as reconstructed physics objects in ATLAS is continuously assessed by inspection of a standard set of distributions, and data-quality flags are recorded in a database for each luminosity block (of about two minutes of data-taking). This analysis selects events satisfying data-quality criteria for the Inner Detector and the calorimeters, and for track, jet, and missing transverse energy reconstruction [39].

For each event, the reconstructed primary vertex position is required to be consistent with the beamspot, both transversely and longitudinally, and to be reconstructed from at least five tracks with transverse momentum $p_T^{\text{track}} > 150$ MeV associated with it. The primary vertex is defined as the one with the highest associated sum of squared track transverse momenta $\Sigma(p_T^{\text{track}})^2$, where the sum runs over all tracks used in the vertex fit. Events are selected by requiring a specific OR combination of inclusive single-jet and dijet calorimeter-based triggers [40, 41]. The combinations are chosen such that the trigger efficiency for each p_T bin is greater than 99%. For the lowest p_T bin (30–40 GeV), this requirement is relaxed, allowing the lowest-threshold calorimeter inclusive single-jet trigger to be used with an efficiency above 95%.

Jets are reconstructed with the anti- k_r jet algorithm [42] using the FastJet software [43] with radius parameters $R = 0.4$ or $R = 0.6$, a four-momentum recombination scheme, and three-dimensional calorimeter topological clusters [44] as inputs. Topological clusters are built from calorimeter cells with a signal at least four times higher than the root-mean-square (RMS) of the noise distribution (seed cells). Cells neighbouring the seed which have a signal to RMS-noise ratio ≥ 2 are then iteratively added. Finally, all nearest neighbour cells are added to the cluster without any threshold.

Jets from non-collision backgrounds (e.g. beam-gas events) and instrumental noise are removed using the selection criteria outlined in Ref. [39].

Jets are categorized according to their reconstructed rapidity in four different regions to account for the differently instrumented parts of the calorimeter:

- Central region ($|y| < 0.8$).
- Extended Tile Barrel ($0.8 \leq |y| < 1.2$).
- Transition region ($1.2 \leq |y| < 2.1$).
- End-Cap region ($2.1 \leq |y| < 2.8$).

Events are selected only if the transverse momenta of the two leading jets are above a jet reconstruction threshold of 7 GeV at the electromagnetic scale (see Section 5) and within $|y| \leq 2.8$, at least one of them being in the central region. The analysis is restricted to $|y| \leq 2.8$ because of the limited number of jets at higher rapidities.

Monte Carlo simulated “particle jets” are defined as those built using the same jet algorithm as described above, but using instead as inputs the stable particles from the event generator (with a lifetime longer than 10 ps), excluding muons and neutrinos.

5 Jet energy calibration

Calorimeter jets are reconstructed from calorimeter energy deposits measured at the electromagnetic scale (EM-scale), the baseline signal scale for the energy deposited by electromagnetic showers in the calorimeter. Their transverse momentum is referred to as $p_T^{\text{EM-scale}}$. For hadrons this leads to a jet energy measurement that is typically 15–55% lower than the true energy, due mainly to the non-compensating nature of the ATLAS calorimeter [45]. The jet response is defined as the ratio of calorimeter jet p_T and particle jet p_T , reconstructed with the same algorithm, and matched in $\eta - \phi$ space (see Section 9).

Fluctuations of the hadronic shower, in particular of its electromagnetic content, as well as energy losses in the dead material lead to a degraded resolution and jet energy measurement compared to particles interacting only electromagnetically. Several complementary jet calibration schemes with different levels of complexity and different sensitivity to systematic effects have been developed to understand the jet energy measurements. The jet calibration is performed by applying corrections derived from Monte Carlo simulations to restore the jet response to unity. This is referred to as determining the jet energy scale (JES).

The analysis presented in this article aims to determine the jet energy resolution for jets reconstructed using various JES strategies. A simple calibration, referred to as the EM+JES calibration scheme, has been chosen for the 2010 data [39]. It allows a direct evaluation of the systematic uncertainties from single-hadron response measurements and is therefore suitable for first physics analyses. More sophisticated calibration techniques to improve the jet resolution and reduce partonic flavour response differences have also been developed. They are the Local Cluster Weighting (LCW), the Global Cell Weighting (GCW) and the Global Sequential (GS) methods [39]. In addition to these calorimeter calibration schemes, a Track-Based Jet Correction (TBJC) has been derived to adjust the response and reduce fluctuations on a jet-by-jet basis without changing the average jet energy scale. These calibration techniques are briefly described below.

5.1 The EM+JES calibration

For the analysis of the first proton-proton collisions, a simple Monte Carlo simulation-based correction is applied as the default to restore the hadronic energy scale on average. The EM+JES calibration scheme applies corrections as a function of the jet transverse momentum and pseudorapidity to jets reconstructed at the electromagnetic scale. The main advantage of this approach is that it allows the most direct evaluation of the systematic uncertainties. The uncertainty on the absolute jet energy scale was determined to be less than $\pm 2.5\%$ in the central calorimeter region ($|\eta| < 0.8$) and $\pm 14\%$ in the most forward region ($3.2 \leq |\eta| < 4.5$) for jets with $p_T > 30$ GeV [39]. These uncertainties were evaluated using test-beam results, single hadron response in situ measurements, comparison with jets built from tracks, p_T balance in dijet and γ +jet events, estimations of pile-up energy deposits, and detailed Monte Carlo comparisons.

5.2 The Local Cluster Weighting (LCW) calibration

The LCW calibration scheme uses properties of clusters to calibrate them individually *prior* to jet finding and reconstruction. The calibration weights are determined from Monte Carlo simulations of charged and neutral pions according to the cluster topology measured in the calorimeter. The cluster properties used are the energy density in the cells forming them, the fraction of their energy deposited in the different calorimeter layers, the cluster isolation and its depth in the calorimeter. Corrections are applied to the cluster energy to account for the energy deposited in the calorimeter but outside of clusters and energy deposited in material before and in between the calorimeters. Jets are formed from calibrated clusters, and a final correction is applied to the jet energy to account for jet-level effects. The resulting jet energy calibration is denoted as LCW+JES.

5.3 The Global Cell Weighting (GCW) calibration

The GCW calibration scheme attempts to compensate for the different calorimeter response to hadronic and electromagnetic energy deposits at cell level. The hadronic signal is characterized by low cell energy densities and, thus, a positive weight is applied. The weights, which depend on the cell energy density and the calorimeter layer only, are determined by minimizing the jet resolution evaluated by comparing reconstructed and particle jets in Monte Carlo simulation. They correct for several effects at once (calorimeter non-compensation, dead material, etc.). A jet-level correction is applied to jets reconstructed from weighted cells to account for global effects. The resulting jet energy calibration is denoted as GCW+JES.

5.4 The Global Sequential (GS) calibration

The GS calibration scheme uses the longitudinal and transverse structure of the jet calorimeter shower to compensate for fluctuations in the jet energy measurement. In this scheme the jet energy response is first calibrated with the EM+JES calibration. Subsequently, the jet properties are used to exploit the topology of the energy deposits in the calorimeter to characterize fluctuations in the hadronic shower development. These corrections are applied such that the mean jet energy is left unchanged, and each correction is applied sequentially. This calibration is designed to improve the jet energy resolution without changing the average jet energy scale.

5.5 Track-based correction to the jet calibration

Regardless of the inputs, algorithms and calibration methods chosen for calorimeter jets, more information on the jet topology can be obtained from reconstructed tracks associated to the jet. Calibrated jets have an average energy response close to unity. However, the energy of an individual jet can be over- or underestimated depending on several factors, for example: the ratio of the electromagnetic and hadronic components of the jet; the fraction of energy lost in dead material, in either the inner detector, the solenoid, the cryostat before the LAr, or the

cryostat between the LAr and the TileCal. The reconstructed tracks associated to the jet are sensitive to some of these effects and therefore can be used to correct the calibration on a jet-by-jet basis.

In the method referred to as Track-Based Jet Correction (TBJC) [45], the response is adjusted depending on the number of tracks associated with the jet. The jet energy response is observed to decrease with jet track multiplicity mainly because the ratio of the electromagnetic to the hadronic component decreases on average as the number of tracks increases. In effect, a low charged-track multiplicity typically indicates a predominance of neutral hadrons, in particular π^0 s which yield electromagnetic deposits in the calorimeter with $R \simeq 1$. A large number of charged particles, on the contrary, signals a more dominant hadronic component, with a lower response due to the non-compensating nature of the calorimeter ($h/e < 1$). The TBJC method is designed to be applied as an option in addition to any JES calibration scheme, since it does not change the overall response, to reduce the jet-to-jet energy fluctuations and improve the resolution.

6 In situ jet resolution measurement using the dijet balance method

Two methods are used in dijet events to measure in situ the fractional jet p_T resolution, $\sigma(p_T)/p_T$, which at fixed rapidity is equivalent to the fractional jet energy resolution, $\sigma(E)/E$. The first method, presented in this section, relies on the approximate scalar balance between the transverse momenta of the two leading jets and measures the sensitivity of this balance to the presence of extra jets directly from data. The second one, presented in the next section, uses the projection of the vector sum of the leading jets' transverse momenta on the coordinate system bisector of the azimuthal angle between the transverse momentum vectors of the two jets. It takes advantage of the very different sensitivities of each of these projections to the underlying physics of the dijet system and to the jet energy resolution.

6.1 Measurement of resolution from asymmetry

The dijet balance method for the determination of the jet p_T resolution is based on momentum conservation in the transverse plane. The asymmetry between the transverse momenta of the two leading jets $A(p_{T,1}, p_{T,2})$ is defined as

$$A(p_{T,1}, p_{T,2}) \equiv \frac{p_{T,1} - p_{T,2}}{p_{T,1} + p_{T,2}}. \quad (1)$$

where $p_{T,1}$ and $p_{T,2}$ refer to the randomly ordered transverse momenta of the two leading jets. The width $\sigma(A)$ of a Gaussian fit to $A(p_{T,1}, p_{T,2})$ is used to characterize the asymmetry distribution and determine the jet p_T resolutions.

For events with exactly two particle jets that satisfy the hypothesis of momentum balance in the transverse plane, and requiring both jets to be in the same rapidity region, the relation between $\sigma(A)$ and the fractional jet resolution is given by

$$\sigma(A) = \frac{\sqrt{\sigma^2(p_{T,1}) + \sigma^2(p_{T,2})}}{\langle p_{T,1} + p_{T,2} \rangle} \simeq \frac{1}{\sqrt{2}} \frac{\sigma(p_T)}{p_T}, \quad (2)$$

where $\sigma(p_{T,1}) = \sigma(p_{T,2}) = \sigma(p_T)$, since both jets are in the same y region.

If one of the two leading jets (j) is in the rapidity bin being probed and the other one (i) in a reference y region, it can be shown that the fractional jet p_T resolution is given by

$$\frac{\sigma(p_T)}{p_T} \Big|_{(j)} = \sqrt{4\sigma^2(A_{(i,j)}) - 2\sigma^2(A_{(i)})}, \quad (3)$$

where $A_{(i,j)}$ is measured in a topology with the two jets in different rapidity regions and where $(i) \equiv (i, i)$ denotes both jets in the same y region.

The back-to-back requirement is approximated by an azimuthal angle cut between the leading jets, $\Delta\phi(j_1, j_2) \geq 2.8$, and a veto on the third jet momentum, $p_{T,3}^{\text{EM-scale}} < 10 \text{ GeV}$, with no rapidity restriction. The resulting asymmetry distribution is shown in Fig. 1 for a $\bar{p}_T \equiv (p_{T,1} + p_{T,2})/2$ bin of $60 \text{ GeV} \leq \bar{p}_T < 80 \text{ GeV}$, in the central region ($|y| < 0.8$). Reasonable agreement in the bulk is observed between data and Monte Carlo simulation.

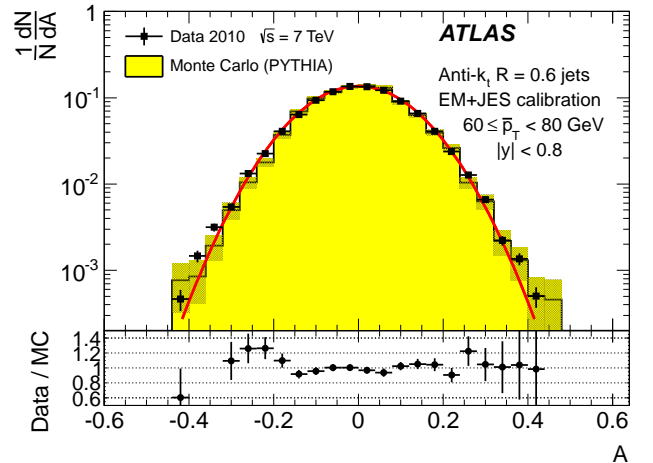


Fig. 1: Asymmetry distribution as defined in Equation (1) for $\bar{p}_T = 60 - 80 \text{ GeV}$ and $|y| < 0.8$. Data (points with error bars) and Monte Carlo simulation (histogram with shaded bands) are overlaid, together with a Gaussian fit to the data. The lower panel shows the ratio between data and MC simulation. The errors shown are only statistical.

6.2 Soft radiation correction

Although requirements on the azimuthal angle between the leading jets and on the third jet transverse momentum are designed to enrich the purity of the back-to-back jet sample, it is important to account for the presence of additional soft particle jets not detected in the calorimeter.

In order to estimate the value of the asymmetry for a pure particle dijet event, $\sigma(p_T)/p_T \equiv \sqrt{2}\sigma(A)$ is recomputed allowing for the presence of an additional third jet in the sample for a series of $p_{T,3}^{\text{EM-scale}}$ cut-off threshold values up to 20 GeV.

The cut on the third jet is placed at the EM-scale to be independent of calibration effects and to have a stable reference for all calibration schemes. For each p_T bin, the jet energy resolutions obtained with the different $p_{T,3}^{\text{EM-scale}}$ cuts are fitted with a straight line and extrapolated to $p_{T,3}^{\text{EM-scale}} \rightarrow 0$, in order to estimate the expected resolution for an ideal dijet topology

$$\frac{\sigma(p_T)}{p_T} \Big|_{p_{T,3}^{\text{EM-scale}} \rightarrow 0}$$

The dependence of the jet p_T resolution on the presence of a third jet is illustrated in Fig. 2. The linear fits and their extrapolations for a \bar{p}_T bin of $60 \leq \bar{p}_T < 80$ GeV are shown. Note that the resolutions become systematically broader as the $p_{T,3}^{\text{EM-scale}}$ cut increases. This is a clear indication that the jet resolution determined from two-jet topologies depends on the presence of additional radiation and on the underlying event.

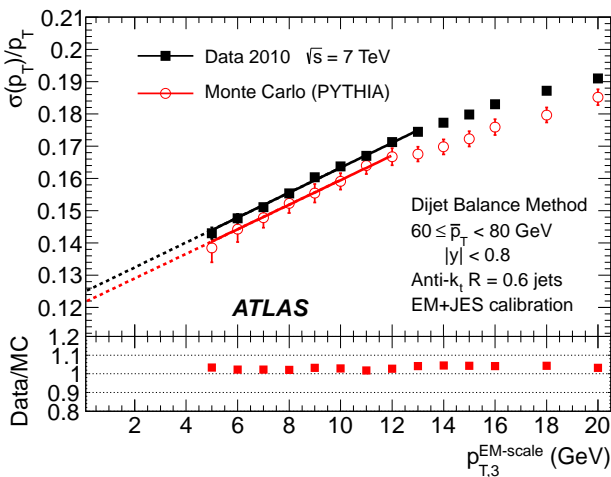


Fig. 2: Fractional jet p_T resolutions, from Equation 2, measured in events with $60 \leq \bar{p}_T < 80$ GeV and with third jet with p_T less than $p_{T,3}^{\text{EM-scale}}$, as a function of $p_{T,3}^{\text{EM-scale}}$, for data (squares) and Monte Carlo simulation (circles). The solid lines correspond to linear fits while the dashed lines show the extrapolations to $p_{T,3}^{\text{EM-scale}} = 0$. The lower panel shows the ratio between data and MC simulation. The errors shown are only statistical.

A soft radiation (SR) correction factor, $K_{\text{soft}}(\bar{p}_T)$, is obtained from the ratio of the values of the linear fit at 0 GeV and at 10 GeV:

$$K_{\text{soft}}(\bar{p}_T) = \frac{\frac{\sigma(p_T)}{p_T} \Big|_{p_{T,3}^{\text{EM-scale}} \rightarrow 0 \text{ GeV}}}{\frac{\sigma(p_T)}{p_T} \Big|_{p_{T,3}^{\text{EM-scale}} = 10 \text{ GeV}}} \quad (4)$$

This multiplicative correction is applied to the resolutions extracted from the dijet asymmetry for $p_{T,3}^{\text{EM-scale}} < 10$ GeV events. The correction varies from 25% for events with \bar{p}_T of 50 GeV down to 5% for \bar{p}_T of 400 GeV. In order to limit the statistical fluctuations, $K_{\text{soft}}(\bar{p}_T)$ is fit with a parameterization

of the form $K_{\text{soft}}(\bar{p}_T) = a + b/(\log \bar{p}_T)^2$, which was found to describe the distribution well, within uncertainties. The differences in the resolution due to other parameterizations were studied and treated as a systematic uncertainty, resulting in a relative uncertainty of about 6% (see Section 10).

6.3 Particle balance correction

The p_T difference between the two calorimeter jets is not solely due to resolution effects, but also to the balance between the respective particle jets,

$$p_{T,2}^{\text{calo}} - p_{T,1}^{\text{calo}} = (p_{T,2}^{\text{calo}} - p_{T,2}^{\text{part}}) - (p_{T,1}^{\text{calo}} - p_{T,1}^{\text{part}}) + (p_{T,2}^{\text{part}} - p_{T,1}^{\text{part}}).$$

The measured difference (left side) is decomposed into resolution fluctuations (the first two terms on the right side) plus a particle-level balance (PB) term that originates from out-of-jet showering in the particle jets and from soft QCD effects. In order to correct for this contribution, the particle-level balance is estimated using the same technique (asymmetry plus soft radiation correction) as for calorimeter jets. The contribution of the dijet PB after the SR correction is subtracted in quadrature from the in situ resolution for both data and Monte Carlo simulation. The result of this procedure is shown for simulated events in the central region in Fig. 3. The relative size of the particle-level balance correction with respect to the measured resolutions varies between 2% and 10%.

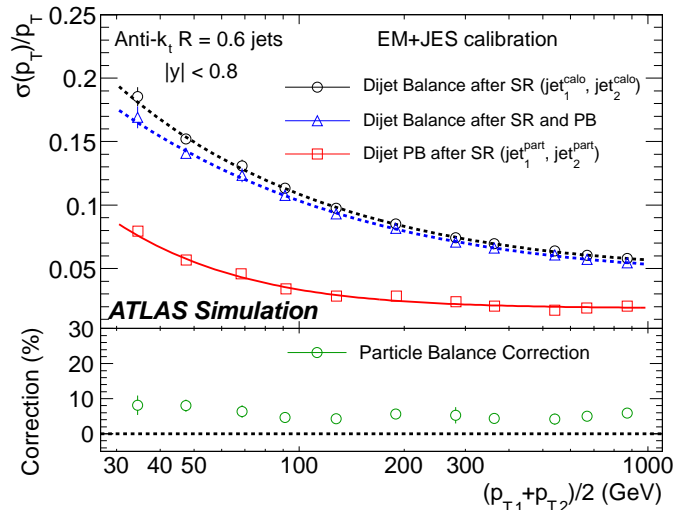


Fig. 3: Fractional jet resolution obtained in simulation using the dijet balance method, shown as a function of \bar{p}_T , both before (circles) and after the particle-balance (PB) correction (triangles). Also shown is the dijet PB correction itself (squares) and, in the lower panel, its relative size with respect to the fractional jet resolution. The errors shown are only statistical.

7 In situ jet resolution measurement using the bisector method

7.1 Bisector rationale

The bisector method [14] is based on a transverse balance vector, \vec{P}_T , defined as the vector sum of the momenta of the two leading jets in dijet events. This vector is projected along an orthogonal coordinate system in the transverse plane, (ψ, η) , where η is chosen in the direction that bisects the angle formed by $\vec{p}_{T,1}$ and $\vec{p}_{T,2}$, $\Delta\phi_{12} = \phi_1 - \phi_2$. This is illustrated in Fig. 4.

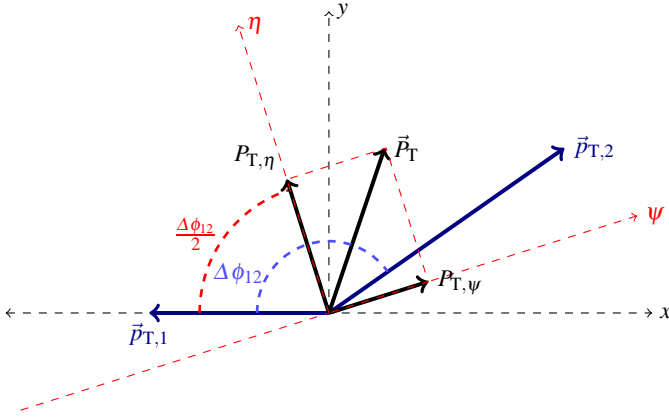


Fig. 4: Variables used in the bisector method. The η -axis corresponds to the azimuthal angular bisector of the dijet system in the plane transverse to the beam, while the ψ -axis is defined as the one orthogonal to the η -axis.

For a perfectly balanced dijet event, $\vec{P}_T = 0$. There are of course a number of sources that give rise to significant fluctuations around this value, and thus to a non-zero variance of its ψ and η components, denoted σ_ψ^2 and σ_η^2 , respectively. At particle level, \vec{P}_T^{part} receives contributions mostly from initial-state radiation. This effect is expected to be isotropic in the (ψ, η) plane, leading to similar fluctuations in both components, $\sigma_\psi^{\text{part}} = \sigma_\eta^{\text{part}}$.

The validity of this assumption, which is at the root of the bisector method, can be checked with Monte Carlo simulations and with data. The precision with which it can be assessed is considered as a systematic uncertainty (see Section 7.2). The ψ component has greater sensitivity to the energy resolution because $P_{T,\psi}$ is the difference between two large transverse momentum components while $P_{T,\eta}$ is the sum of two small components. Effects such as contamination from 3-jet events or final-state radiation not absorbed in the leading jets by the clustering algorithm could give rise to a $\sigma_\psi^{\text{part}} > \sigma_\eta^{\text{part}}$. At calorimeter level, $\sigma_\psi^{\text{calo}}$ is expected to be significantly larger than $\sigma_\eta^{\text{calo}}$, mostly because of the jet energy resolution.

If both jets belong to the same y region, such that they have the same average jet energy resolution, it can be shown that

$$\frac{\sigma(p_T)}{p_T} = \frac{\sqrt{\sigma_\psi^{\text{calo}2} - \sigma_\eta^{\text{calo}2}}}{\sqrt{2} p_T \sqrt{\langle |\cos \Delta\phi_{12}| \rangle}}. \quad (5)$$

The resolution is thus expressed in terms of calorimeter observables only. The contribution from soft radiation and the underlying event is minimised by subtracting in quadrature σ_η from σ_ψ .

If one of the leading jets (j) belongs to the rapidity region being probed, and the other one (i) to a previously measured reference y region, then

$$\frac{\sigma(p_T)}{p_T} \Big|_{(j)} = \sqrt{\frac{\sigma_\psi^{\text{calo}2} - \sigma_\eta^{\text{calo}2}}{p_T^2 \langle |\cos \Delta\phi_{12}| \rangle} \Big|_{(i,j)} - \frac{\sigma^2(p_T)}{p_T^2} \Big|_{(i)}}. \quad (6)$$

The dispersions σ_ψ and σ_η are extracted from Gaussian fits to the $P_{T,\psi}$ and $P_{T,\eta}$ distributions in bins of \bar{p}_T . There is no $\Delta\phi$ cut imposed between the leading jets, but it is implicitly limited by a $p_{T,3}^{\text{EM-scale}} < 10$ GeV requirement on the third jet, as discussed in the next section. Figure 5 compares the distributions of $P_{T,\psi}$ and $P_{T,\eta}$ between data and Monte Carlo simulation in the momentum bin $60 \leq \bar{p}_T < 80$ GeV. The distributions agree within statistical fluctuations. The resolutions obtained from the $P_{T,\psi}$ and $P_{T,\eta}$ components of the balance vector are summarised in the central region as a function of \bar{p}_T in Fig. 6. As expected, the resolution on the η component does not vary with the jet p_T , while the resolution on the ψ component degrades as the jet p_T increases.

7.2 Validation of the soft radiation isotropy with data

Figure 7 shows the width of the ψ and η components of \vec{P}_T as a function of the $p_{T,3}^{\text{EM-scale}}$ cut, for anti- k_t jets with $R = 0.6$. The two leading jets are required to be in the same rapidity region, $|y| < 0.8$, while there is no rapidity restriction for the third jet. As expected, both components increase due to the contribution from soft radiation as the $p_{T,3}$ cut is increased. Also shown as a function of the $p_{T,3}^{\text{EM-scale}}$ cut is the square-root of the difference between their variances, which yields the fractional momentum resolution when divided by $2 \langle p_T^2 \rangle \langle \cos \Delta\phi \rangle$.

It is observed that the increase of the soft radiation contribution to $\sigma_\psi^{\text{calo}}$ and $\sigma_\eta^{\text{calo}}$ cancels in the squared difference and that it remains almost constant, within statistical uncertainties, up to $p_{T,3}^{\text{EM-scale}} \simeq 20$ GeV for \bar{p}_T between 160-260 GeV. The same behaviour is observed for other \bar{p}_T ranges. This cancellation demonstrates that the isotropy assumption used for the bisector method is valid over a wide range of choices of $p_{T,3}^{\text{EM-scale}}$ without the need for requiring an explicit $\Delta\phi$ cut between the leading jets. The precision with which it can be ascertained in situ that $\sigma_\psi^{\text{part}} = \sigma_\eta^{\text{part}}$ is taken conservatively as a systematic uncertainty on the method, of about 4–5% at 50 GeV (see Section 10).

8 Performance for the EM+JES calibration

The performances of the dijet balance and bisector methods are compared for both data and Monte Carlo simulation as a function of jet p_T for jets reconstructed in the central region with the anti- k_t algorithm with $R = 0.6$ and using the EM+JES calibration scheme. The results are shown in Fig. 8. The resolutions obtained from the two independent in situ methods are in

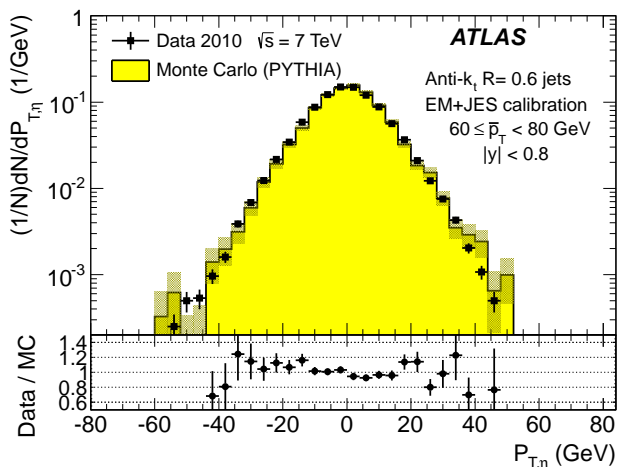
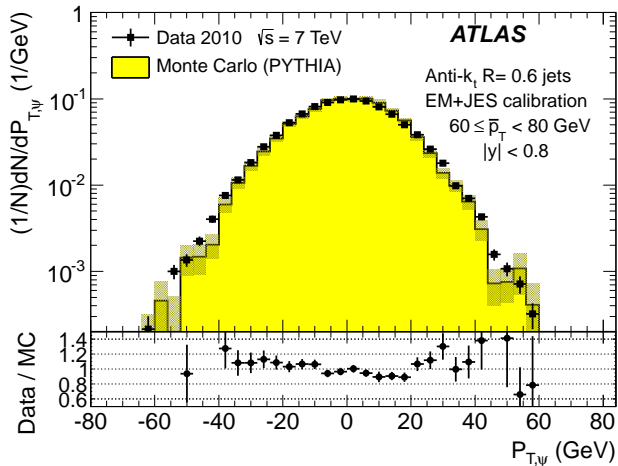


Fig. 5: Distributions of the $P_{T,\psi}$ (top) and $P_{T,\eta}$ (bottom) components of the balance vector \vec{P}_T , for $\bar{p}_T = 60 - 80$ GeV. The data (points with error bars) and Monte Carlo simulation (histogram with shaded bands) are overlaid. The lower panel shows the ratio between data and MC simulation. The errors shown are only statistical.

good agreement with each other within the statistical uncertainties. The agreement between data and Monte Carlo simulation is also good with some deviations observed at low p_T .

The resolutions for the three jet rapidity bins with $|y| > 0.8$, the Extended Tile Barrel, the Transition and the End-Cap regions, are measured using Eqs. 3 and 6, taking the central region as the reference. The results for the bisector method are shown in Fig. 9. Within statistical errors the resolutions obtained for data and Monte Carlo simulation are in agreement within $\pm 10\%$ over most of the p_T -range in the various regions.

Figure 9 shows that dependences are well described by fits to the standard functional form expected for calorimeter-based resolutions, with three independent contributions, the effective noise (N), stochastic (S) and constant (C) terms.

$$\frac{\sigma(p_T)}{p_T} = \frac{N}{p_T} \oplus \frac{S}{\sqrt{p_T}} \oplus C. \quad (7)$$

The N term is due to external noise contributions that are not (or only weakly) dependent on the jet p_T , and include the electron-

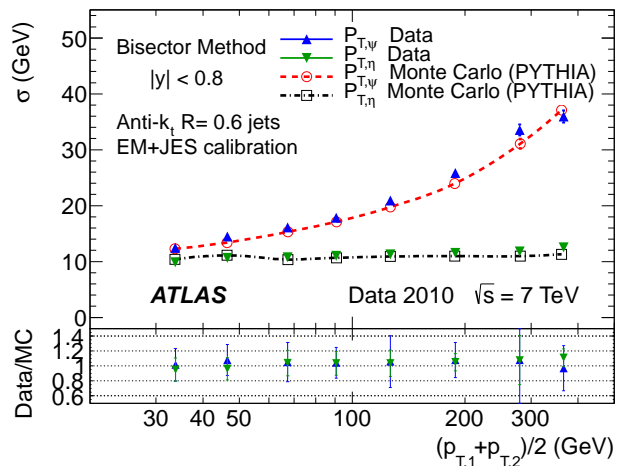


Fig. 6: Standard deviations of $P_{T,\psi}$ and $P_{T,\eta}$, the components of the balance vector, as a function of \bar{p}_T . The lower panel shows the ratio between data and MC simulation. The errors shown are only statistical.

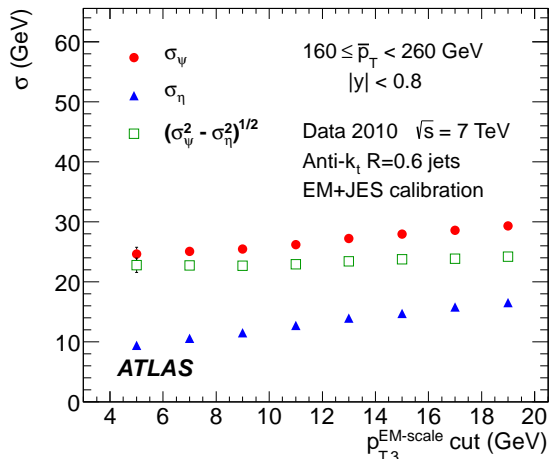


Fig. 7: Standard deviations $\sigma_\psi^{\text{calo}}$, $\sigma_\eta^{\text{calo}}$ and $[(\sigma_\psi^2 - \sigma_\eta^2)^{\text{calo}}]^{1/2}$ as a function of the upper $p_{T,3}^{\text{EM-scale}}$ cut, for $R=0.6$ anti- k_t jets with $\bar{p}_T = 160 - 260$ GeV. The errors shown are only statistical.

ics and detector noise, and contributions from pile-up. It is expected to be significant in the low- p_T region, below ~ 30 GeV. The C term encompasses the fluctuations that are a constant fraction of the jet p_T , assumed at this early stage of data-taking to be due to real signal lost in passive material (e.g. cryostats and solenoid coil), to non-uniformities of response across the calorimeter, etc. It is expected to dominate the high- p_T region, above 400 GeV. For intermediate values of the jet p_T , the statistical fluctuations, represented by the S term, become the limiting factor in the resolution. With the present data sample that covers a restricted p_T range, $30 \text{ GeV} \leq p_T < 500 \text{ GeV}$, there is a high degree of correlation between the fitted parameters and it is not possible to unequivocally disentangle their contributions.

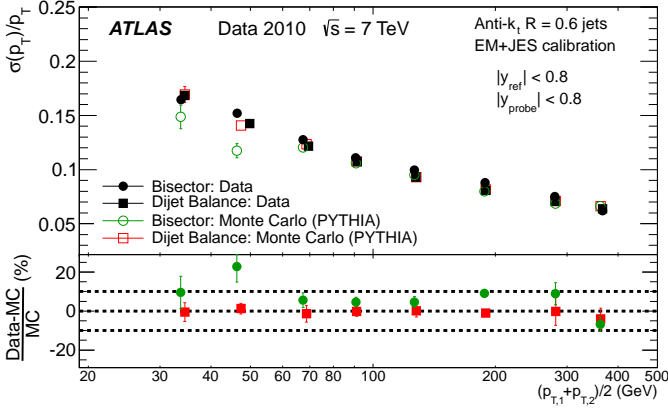


Fig. 8: Fractional jet p_T resolution for the dijet balance and bisector methods as a function of \bar{p}_T . The lower panel shows the relative difference between data and Monte Carlo results. The dotted lines indicate a relative difference of $\pm 10\%$. Both methods are found to be in agreement within 10% between data and Monte Carlo simulation. The errors shown are only statistical.

9 Closure test using Monte Carlo simulation

The Monte Carlo simulation expected resolution is derived considering matched particle and calorimeter jets in the event, with no back-to-back geometry requirements. Matching is done in $\eta - \phi$ space, and jets are associated if $\Delta R = \sqrt{(\Delta\eta)^2 + (\Delta\phi)^2} < 0.3$. The jet response is defined as $p_T^{\text{calo}}/p_T^{\text{part}}$, in bins of p_T^{part} , where p_T^{calo} and p_T^{part} correspond to the transverse momentum of the reconstructed jet and its matched particle jet, respectively. The jet response distribution is modelled with a Gaussian fit, and its standard deviation is defined as the truth jet p_T resolution.

The Monte Carlo simulation truth jet p_T resolution is compared to the results obtained from the dijet balance and the bisector in situ methods (applied to Monte Carlo simulation) in Fig. 10. The agreement between the three sets of points is within 10%. This result confirms the validity of the physical assumptions discussed in Sections 6 and 7 and the inference that the observables derived for the in situ MC dijet balance and bisector methods provide reliable estimates of the jet energy resolution. The systematic uncertainties on these estimates are of the order of 10% (15%) for jets with $R = 0.6$ ($R = 0.4$), and are discussed in Section 10.

10 Jet energy resolution uncertainties

10.1 Experimental uncertainties

The squares (circles) in Fig. 11 show the experimental relative systematic uncertainty in the dijet balance (bisector) method as a function of \bar{p}_T . The different contributions are discussed below. The shaded area corresponds to the larger of the two systematic uncertainties for each \bar{p}_T bin.

For the dijet balance method, systematic uncertainties take into account the variation in resolution when applying different $\Delta\phi$ cuts (varied from 2.6 to 3.0), resulting in a 2–3% effect for

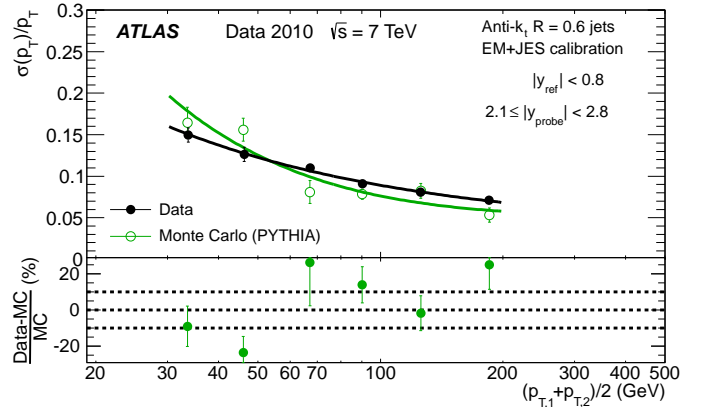
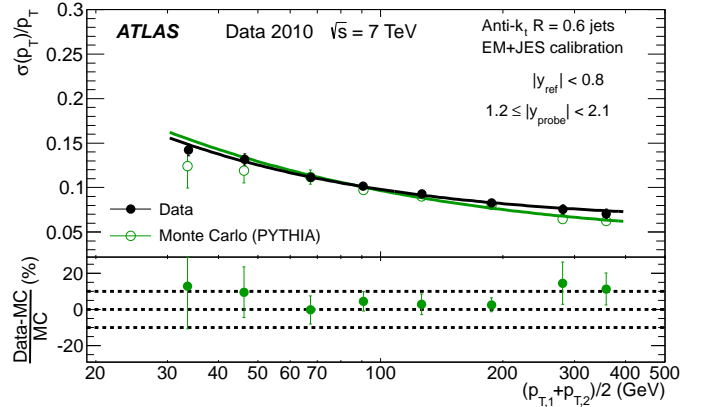
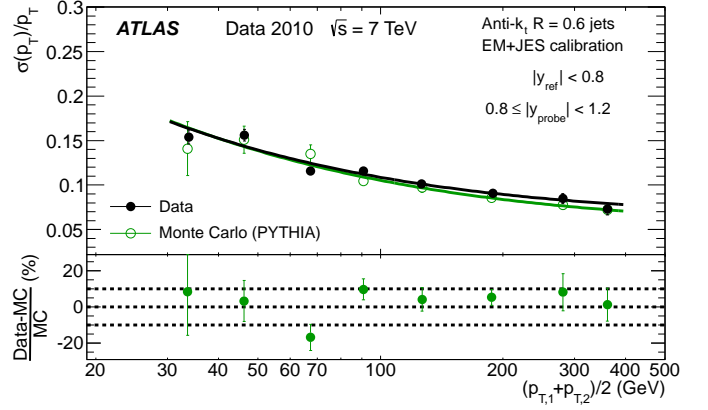


Fig. 9: Fractional jet p_T resolution as a function of \bar{p}_T for anti- k_t with $R = 0.6$ jets in the Extended Tile Barrel (top), Transition (center) and End-Cap (bottom) regions using the bisector method. In the lower panel of each figure, the relative difference between the data and the MC simulation results is shown. The dotted lines indicate a relative difference of $\pm 10\%$. The errors shown are only statistical.

$p_T = 30\text{--}60$ GeV, and when varying the soft radiation correction modelling, which contributes up to 6% at $p_T \approx 30$ GeV. For the bisector method, the relative systematic uncertainty is about 4–5%, and is derived from the precision with which the assumption that $\sigma_{\psi}^{\text{part}} = \sigma_{\eta}^{\text{part}}$ when varying the $p_{T,3}^{\text{EM-scale}}$ cut can be verified.

The contribution from the JES uncertainties [39] is 1–2%, determined by re-calculating the jet resolutions after varying

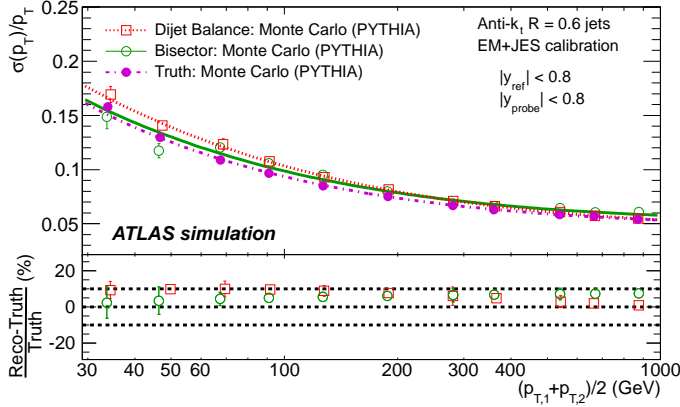


Fig. 10: Comparison between the Monte Carlo simulation truth jet p_T resolution and the results obtained from the bisector and dijet balance in situ methods (applied to Monte Carlo simulation) for the EM+JES calibration, as a function of \bar{p}_T . The lower panel of the figure shows the relative difference, obtained from the fits, between the in situ methods and Monte Carlo truth results. The dotted lines indicate a relative difference of $\pm 10\%$. The errors shown are only statistical.

the JES within its uncertainty in a fully correlated way. The resolution has also been studied in simulated events with added pile-up events (i.e. additional interactions as explained in Section 3.3), as compared to events with one hard interaction only. The sensitivity of the resolution to pile-up is found to be less than 1% for an average number of vertices per event of 1.9.

In summary, the overall relative uncertainty from the in situ methods decreases from about 7% at $p_T = 30$ GeV down to 4% at $p_T = 500$ GeV. Figure 11 also shows in dashed lines the absolute value of the relative difference between the two in situ methods, for both data and Monte Carlo simulation. They are found to be in agreement within 4% up to 500 GeV, and consistent with these systematic uncertainties.

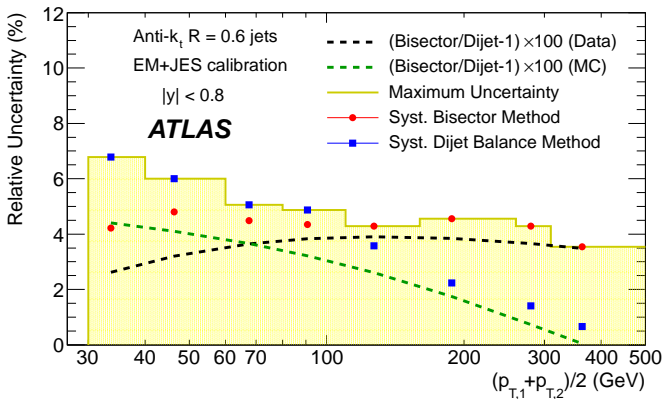


Fig. 11: The experimental systematic uncertainty on the dijet balance (squares) and bisector (circles) methods as a function of \bar{p}_T , for jets with $|y| < 0.8$. The absolute value of the relative difference between the two methods in each p_T bin is also shown for data and for Monte Carlo simulation (dashed lines).

10.2 Uncertainties due to the event modelling in the Monte Carlo generators

The expected jet p_T resolution is calculated for other Monte Carlo simulations in order to assess its dependence on different generator models (ALPGEN and HERWIG++), PYTHIA tunes (PERUGIA2010), and other systematic variations (PARP90; see Sec. 3.1). Differences between the nominal Monte Carlo simulation and PYTHIA8 [24] have also been considered. These effects, displayed in Fig. 12, never exceed 4%. Although they are not relevant for the in situ measurements of the jet energy resolution themselves, physics analyses sensitive to the expected resolution have to consider a systematic uncertainty from event modelling estimated from the sum in quadrature of the different cases considered here. This is shown by the shaded area in Fig. 12 and found to be at most 5%.

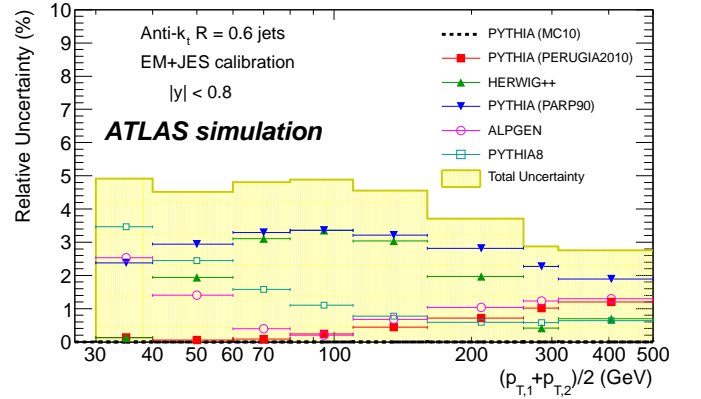


Fig. 12: Systematic uncertainty due to event modelling in Monte Carlo generators on the expected jet energy resolution as a function of p_T , for jets with $|y| < 0.8$. The reference is taken from PYTHIA MC10 and other event generators are shown as solid triangles (HERWIG++) and open circles (ALPGEN). Solid squares (PYTHIA PERUGIA2010) and inverted triangles (PYTHIA PARP90) summarize differences coming from different tunes and cut-off parameters, respectively. Open squares compare the nominal simulation with PYTHIA8.

10.3 Uncertainties on the measured resolutions

The uncertainties in the measured resolutions are dominated by the systematic uncertainties, which are shown in Table 1 as a percentage of the resolution for the four rapidity regions and the two jet sizes considered, and for characteristic ranges, low (~ 50 GeV), medium (~ 150 GeV) and high (~ 400 GeV) p_T . The results are similar for the four calibration schemes. The dominant sources of systematic uncertainty are the closure and the data/MC agreement. The closure uncertainty (see Section 9), defined as the precision with which in simulation the resolution determined using the in situ method reproduces the truth jet resolution, is larger for $R = 0.4$ than for $R = 0.6$, decreases with p_T , and is basically independent of the rapidity.

| Jet radius | Rapidity range | Total systematic uncertainty | | |
|------------|----------------------|------------------------------|-----------|------------|
| | | Low p_T | Med p_T | High p_T |
| $R = 0.6$ | $0 \leq y < 0.8$ | 12% | 10% | 11% |
| | $0.8 \leq y < 1.2$ | 12% | 10% | 13% |
| | $1.2 \leq y < 2.1$ | 14% | 12% | 14% |
| | $2.1 \leq y < 2.8$ | 15% | 13% | 18% |
| $R = 0.4$ | $0 \leq y < 0.8$ | 17% | 15% | 11% |
| | $0.8 \leq y < 1.2$ | 20% | 18% | 14% |
| | $1.2 \leq y < 2.1$ | 20% | 18% | 14% |
| | $2.1 \leq y < 2.8$ | 20% | 18% | 18% |

Table 1: Relative systematic uncertainties at low (~ 50 GeV), medium (~ 150 GeV) and high (~ 400 GeV) p_T , for the four rapidity regions and the two jet radii studied. The uncertainties are similar for the four calibration schemes.

The data/MC agreement uncertainty is observed to be independent of R , larger at low and high p_T than at medium p_T , and to grow with rapidity because of the increasingly limited statistical accuracy with which checks can be performed to assess it. Other systematic uncertainties are significantly smaller. They include the validity of the soft radiation hypothesis, the jet energy scale uncertainty and the dependence on the number of pile-up interactions. The uncertainty due to event modelling is

not included, as it does not contribute to the in situ measurement itself.

The systematic uncertainties in Table 1 for jets with $R = 0.4$ are dominated by the contribution from the closure test. They decrease with p_T and are constant for the highest three rapidity bins. They are also consistently larger than for the $R = 0.6$ case. The systematic uncertainties for jets with $R = 0.6$ receive comparable contributions from closure and data/MC agreement. They tend to increase with rapidity and are slightly lower in the medium p_T range. The uncertainty increases at high p_T for the end-cap, $2.1 \leq |y| < 2.8$, because of the limited number of events in this region.

11 Jet energy resolution for other calibration schemes

The resolution performance for anti- k_t jets with $R = 0.6$ reconstructed from calorimeter topological clusters for the Local Cluster Weighting (LCW+JES), the Global Cell Weighting (GCW+JES) and the Global Sequential (GS) calibration strategies (using the bisector method) is presented in Fig. 13 for the Central, Extended Tile Barrel, Transition and End-Cap regions. The top part shows the resolutions determined from

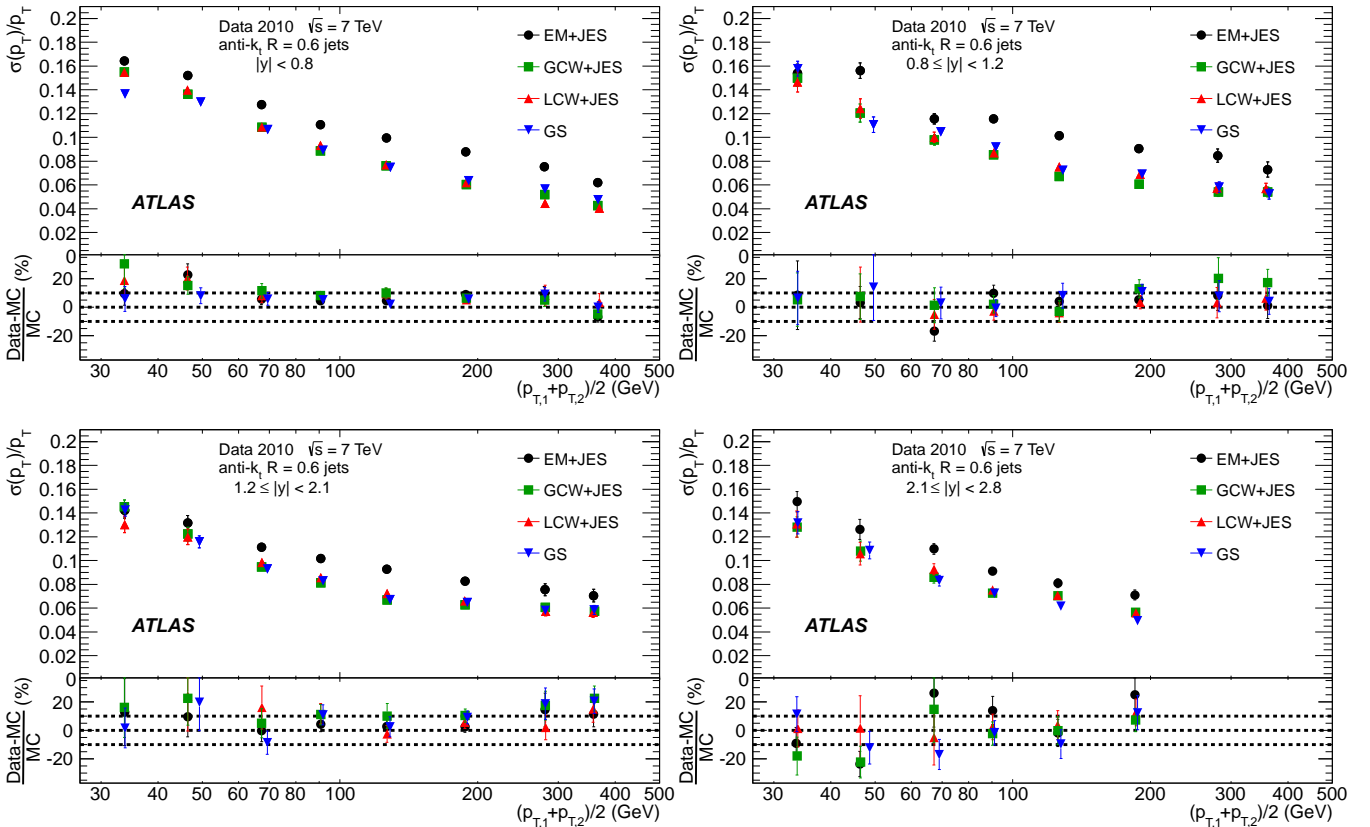


Fig. 13: Fractional jet p_T resolutions as a function of \bar{p}_T for anti- k_t jets with $R = 0.6$ with $|y| < 0.8$ (top left), $0.8 \leq |y| < 1.2$ (top right), $1.2 \leq |y| < 2.1$ (bottom left) and $2.1 \leq |y| < 2.8$ (bottom right), using the bisector in situ method, for four jet calibration schemes: EM+JES, Local Cluster Weighting (LCW+JES), Global Cell Weighting (GCW+JES) and Global Sequential (GS). The lower panels show the relative difference between data and Monte Carlo simulation results. The dotted lines indicate relative differences of $\pm 10\%$. The errors shown are only statistical.

data, whereas the bottom part compares data and Monte Carlo simulation results. The relative improvement in resolution with respect to the EM+JES calibrated jets is comparable for the three more sophisticated calibration techniques. It ranges from 10% at low p_T up to 40% at high p_T for all four rapidity regions.

Figure 14 displays the resolutions for the two in situ methods applied to data and Monte Carlo simulation for $|y| < 0.8$ (left plots). It can be observed that the results from the two methods agree, within uncertainties. The Monte Carlo simula-

tion reproduces the data within 10%. The figures on the right show the results of a study of the closure for each case, where the truth resolution is compared to that obtained from the in situ methods applied to Monte Carlo simulation data. The agreement is within 10%. Overall, comparable agreement in resolution is observed in data and Monte Carlo simulation for the EM+JES, LCW+JES, GCW+JES and GS calibration schemes, with similar systematic uncertainties in the resolutions determined using in situ methods.

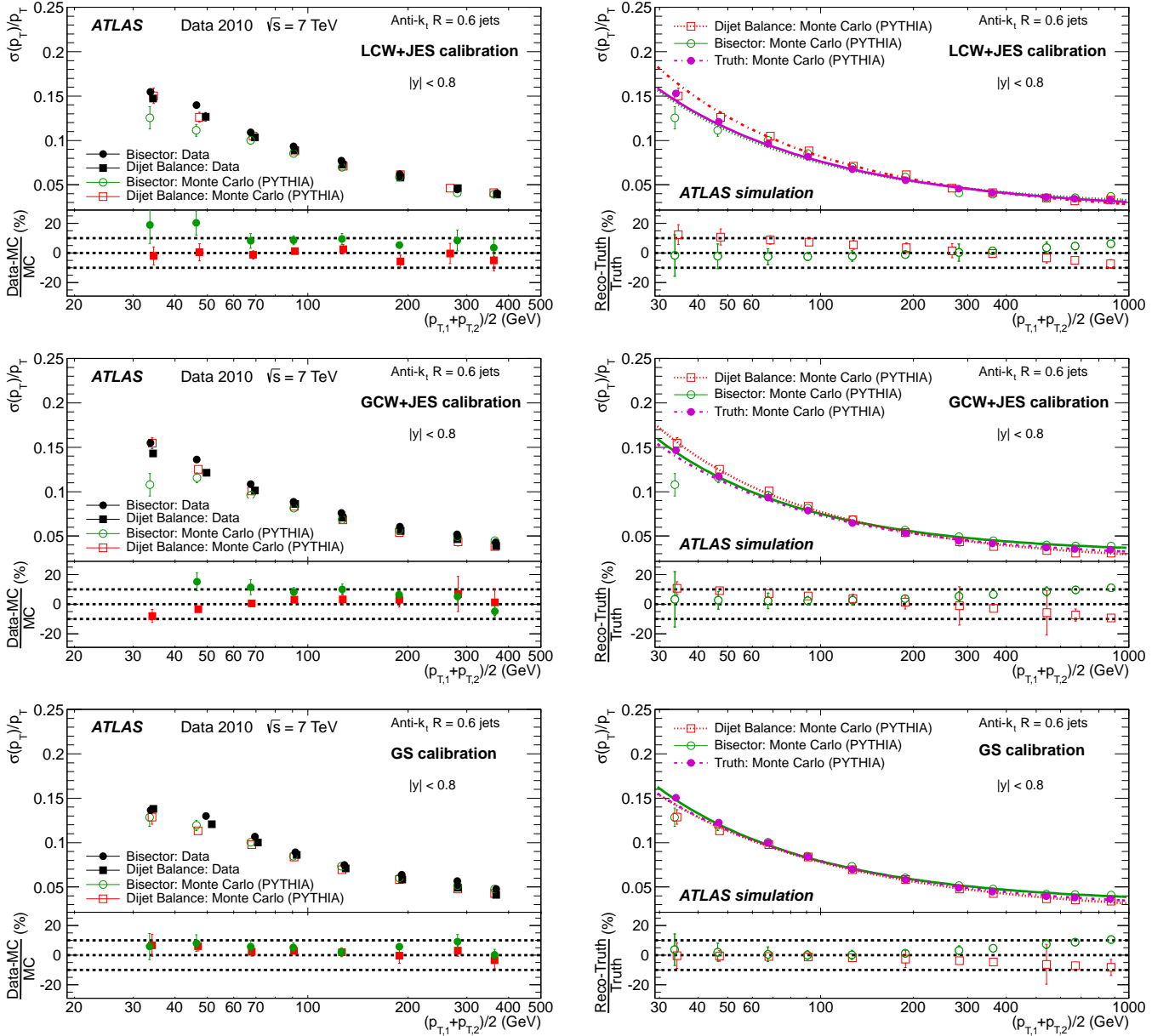


Fig. 14: Fractional jet p_T resolutions as a function of \bar{p}_T for anti- k_t jets with $R = 0.6$ for the Local Cluster Weighting (LCW+JES), Global Cell Weighting (GCW+JES) and Global Sequential (GS) calibrations. *Left*: Comparison of both in situ methods on data and MC simulation for $|y| < 0.8$. The lower panels show the relative difference. *Right*: Comparison between the Monte Carlo simulation truth jet p_T resolution and the final results obtained from the bisector and dijet balance in situ methods (applied to Monte Carlo simulation). The lower panels show the relative differences, obtained from the fits, between the in situ methods and Monte Carlo truth results. The dotted lines indicate relative differences of $\pm 10\%$. The errors shown are only statistical.

12 Improvement in jet energy resolution using tracks

The addition of tracking information to the calorimeter-based energy measurement is expected to compensate for the jet-by-jet fluctuations and improve the jet energy resolution (see Section 5.5). The performance of the Track-Based Jet Correction method (TBJC) is studied by applying it to both the EM+JES and LCW+JES calibration schemes, in the central region. The measured resolution for anti- k_t jets with $R = 0.6$ ($R = 0.4$) is presented as a function of the average jet transverse momentum in the top (bottom) plot of Fig. 15.

The relative improvement in resolution due to the addition of tracking information is larger at low p_T and more important for the EM+JES calibration scheme. It ranges from 22% (10%) at low p_T to 15% (5%) at high p_T for the EM+JES (LCW+JES) calibration. For $p_T < 70$ GeV, jets calibrated with the EM+JES+TBJC scheme show a similar performance to those calibrated with the LCW+JES+TBJC scheme. Overall, jets with LCW+JES+TBJC show the best fractional energy resolution over the full p_T range.

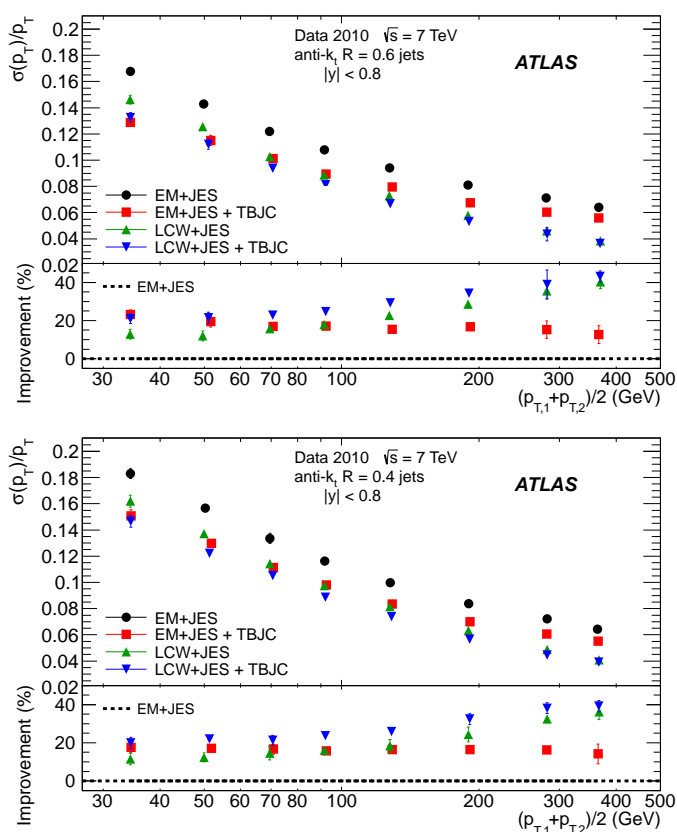


Fig. 15: *Top*: Fractional jet p_T resolutions as a function \bar{p}_T , measured in data for anti- k_t jets with $R = 0.6$ (top) and $R = 0.4$ (bottom) and for four jet calibration schemes: EM+JES, EM+JES+TBJC, LCW+JES and LCW+JES+TBJC. The lower panel of the figure shows the relative improvement for the EM+JES+TBJC, LCW+JES and LCW+JES+TBJC calibrations with respect to the EM+JES jet calibration scheme, used as reference (dotted line). The errors shown are only statistical.

13 Summary

The jet energy resolution for various JES calibration schemes has been measured using two in situ methods with a data sample corresponding to an integrated luminosity of 35 pb^{-1} collected in 2010 by the ATLAS experiment at $\sqrt{s} = 7 \text{ TeV}$.

The Monte Carlo simulation describes the jet energy resolution measured in data within 10% for jets with p_T values between 30 GeV and 500 GeV in the rapidity range $|y| < 2.8$.

The resolutions obtained applying the in situ techniques to Monte Carlo simulation are in agreement within 10% with the resolutions determined by comparing jets at calorimeter and particle level. Overall, the results measured with the two in situ methods have been found to be consistent within systematic uncertainties.

14 Acknowledgements

We thank CERN for the very successful operation of the LHC, as well as the support staff from our institutions without whom ATLAS could not be operated efficiently.

We acknowledge the support of ANPCyT, Argentina; YerPhI, Armenia; ARC, Australia; BMWF and FWF, Austria; ANAS, Azerbaijan; SSTC, Belarus; CNPq and FAPESP, Brazil; NSERC, NRC and CFI, Canada; CERN; CONICYT, Chile; CAS, MOST and NSFC, China; COLCIENCIAS, Colombia; MSMT CR, MPO CR and VSC CR, Czech Republic; DNRF, DNSRC and Lundbeck Foundation, Denmark; EPLANET and ERC, European Union; IN2P3-CNRS, CEA-DSM/IRFU, France; GNSF, Georgia; BMBF, DFG, HGF, MPG and AvH Foundation, Germany; GSRT, Greece; ISF, MINERVA, GIF, DIP and Benoziyo Center, Israel; INFN, Italy; MEXT and JSPS, Japan; CNRST, Morocco; FOM and NWO, Netherlands; BRF and RCN, Norway; MNiSW, Poland; GRICES and FCT, Portugal; MERYS (MECTS), Romania; MES of Russia and ROSATOM, Russian Federation; JINR; MSTB, Serbia; MSSR, Slovakia; ARRS and MVZT, Slovenia; DST/NRF, South Africa; MICINN, Spain; SRC and Wallenberg Foundation, Sweden; SER, SNSF and Cantons of Bern and Geneva, Switzerland; NSC, Taiwan; TAEK, Turkey; STFC, the Royal Society and Leverhulme Trust, United Kingdom; DOE and NSF, United States of America.

The crucial computing support from all WLCG partners is acknowledged gratefully, in particular from CERN and the ATLAS Tier-1 facilities at TRIUMF (Canada), NDGF (Denmark, Norway, Sweden), CC-IN2P3 (France), KIT/GridKA (Germany), INFN-CNAF (Italy), NL-T1 (Netherlands), PIC (Spain), ASGC (Taiwan), RAL (UK) and BNL (USA) and in the Tier-2 facilities worldwide.

References

1. ATLAS Collaboration, *Measurement of inclusive jet and dijet cross sections in proton-proton collisions at 7 TeV centre-of-mass energy with the ATLAS detector*, *Eur.Phys.J.* **C71** (2011) 1512, [arXiv:1009.5908](https://arxiv.org/abs/1009.5908) [[hep-ex](#)].
2. ATLAS Collaboration, *Measurement of Dijet Azimuthal Decorrelations in pp Collisions at $\sqrt{s}=7 \text{ TeV}$* , *Phys. Rev. Lett.* **106** (2011) 172002, [arXiv:1102.2696](https://arxiv.org/abs/1102.2696) [[hep-ex](#)].

3. ATLAS Collaboration, *Measurement of multi-jet cross sections in proton-proton collisions at a 7 TeV center-of-mass energy*, *Eur.Phys.J.* **C71** (2011) 1763, [arXiv:1107.2092 \[hep-ex\]](#).
4. ATLAS Collaboration, *Measurement of the production cross section for W-bosons in association with jets in pp collisions at $\sqrt{s} = 7$ TeV with the ATLAS detector*, *Phys. Lett.* **B 698** (2011) 325–345, [arXiv:1012.5382 \[hep-ex\]](#).
5. ATLAS Collaboration, *Measurement of the top quark-pair production cross section with ATLAS in pp collisions at $\sqrt{s} = 7$ TeV*, *Eur.Phys.J.* **C71** (2011) 1, [arXiv:1012.1792 \[hep-ex\]](#).
6. ATLAS Collaboration, *Search for New Particles in Two-Jet Final States in 7 TeV Proton-Proton Collisions with the ATLAS Detector at the LHC*, *Phys. Rev. Lett.* **105** (2010) 161801, [arXiv:1008.2461 \[hep-ex\]](#).
7. ATLAS Collaboration, *Search for New Physics in Dijet Mass and Angular Distributions in pp Collisions at $\sqrt{s} = 7$ TeV Measured with the ATLAS Detector*, *New J.Phys.* **13** (2011) 053044, [arXiv:1103.3864 \[hep-ex\]](#).
8. ATLAS Collaboration, *Search for supersymmetry using final states with one lepton, jets, and missing transverse momentum with the ATLAS detector in $\sqrt{s} = 7$ TeV pp collisions*, *Phys. Rev. Lett.* **106** (2011) 131802, [arXiv:1102.2357 \[hep-ex\]](#).
9. ATLAS Collaboration, *Search for squarks and gluinos using final states with jets and missing transverse momentum with the ATLAS detector in $\sqrt{s} = 7$ TeV proton-proton collisions*, *Phys.Lett.* **B701** (2011) 186–203, [arXiv:1102.5290 \[hep-ex\]](#).
10. ATLAS Collaboration, *The ATLAS Experiment at the CERN Large Hadron Collider*, *JINST* **3** (2008) S08003.
11. ATLAS Collaboration, *ATLAS Detector Technical Design Report*, CERN-LHCC-99-14, ATLAS-TDR-14. <http://inspirehep.net/record/511648>.
12. L. Evans and P. Bryant, *LHC Machine*, *JINST* **3** (2008) S08001.
13. DØ Collaboration, B. Abbott et al., *High- p_T jets in $p\bar{p}$ collisions at $\sqrt{s} = 630$ GeV and 1800 GeV*, *Phys. Rev.* **D64** (2001) 032003, [arXiv:0012046 \[hep-ex\]](#).
14. UA2 Collaboration, P. Bagnaia et al., *Measurement of jet production properties at the CERN $p\bar{p}$ collider*, *Phys. Lett.* **B 144** (1984) 283.
15. T. Sjostrand, S. Mrenna, and P. Z. Skands, *PYTHIA 6.4 Physics and Manual*, *JHEP* **05** (2006) 026, [arXiv:0603175 \[hep-ph\]](#).
16. R. Corke and T. Sjostrand, *Improved Parton Showers at Large Transverse Momenta*, *Eur.Phys.J.* **C69** (2010) 1–18, [arXiv:1003.2384 \[hep-ph\]](#).
17. T. Sjostrand and P. Z. Skands, *Transverse-momentum-ordered showers and interleaved multiple interactions*, *Eur.Phys.J.* **C39** (2005) 129–154, [arXiv:0408302 \[hep-ph\]](#).
18. B. Andersson et al., *Parton Fragmentation and String Dynamics*, *Phys. Rep.* **97** (1983) 31–145.
19. A. Sherstnev and R. S. Thorne, *Parton distributions for LO generators*, *Eur.Phys.J.* **C55** (2008) 553–575, [arXiv:0711.2473 \[hep-ph\]](#).
20. ATLAS Collaboration, *Charged-particle multiplicities in pp interactions measured with the ATLAS detector at the LHC*, *New J.Phys.* **13** (2011) 053033, [arXiv:1012.5104 \[hep-ex\]](#).
21. P. Z. Skands, *Tuning Monte Carlo Generators: The Perugia Tunes*, *Phys. Rev. D* **82** (2010) 074018, [arXiv:1005.3457 \[hep-ph\]](#).
22. ATLAS Collaboration, *Study of Jet Shapes in Inclusive Jet Production in pp Collisions at $\sqrt{s} = 7$ TeV using the ATLAS Detector*, *Phys.Rev.* **D83** (2011) 052003, [arXiv:1101.0070 \[hep-ex\]](#).
23. ATLAS Collaboration, *ATLAS Monte Carlo tunes for MC09*, ATLAS-PHYS-PUB-2010-002. <http://cdsweb.cern.ch/record/1247375>.
24. T. Sjostrand, *PYTHIA 8 Status Report*, [arXiv:0809.0303 \[hep-ph\]](#).
25. M. Bahr et al., *Herwig++ Physics and Manual*, *Eur.Phys.J.* **C58** (2008) 639–707, [arXiv:0803.0883 \[hep-ph\]](#).
26. G. Corcella et al., *HERWIG 6.5 release note*, [arXiv:0210213 \[hep-ph\]](#).
27. G. Marchesini et al., *A Monte Carlo Event Generator For Simulating Hadron Emission Reactions With Interfering Gluons*, *Comput. Phys. Commun.* **67** (1991) 465–508.
28. G. Marchesini et al., *Monte Carlo Simulation of General Hard Processes with Coherent QCD Radiation*, *Nucl. Phys.* **B 310** (1988) 461.
29. B. R. Webber, *A QCD model for jet fragmentation including soft gluon interference*, *Nucl. Phys.* **B 238** (1984) 492.
30. M. Bahr, S. Gieseke, and M. H. Seymour, *Simulation of multiple partonic interactions in Herwig++*, *JHEP* **07** (2008) 076, [arXiv:0803.3633 \[hep-ph\]](#).
31. M. L. Mangano, M. Moretti, F. Piccinini, R. Pittau, and A. D. Polosa, *ALPGEN, a generator for hard multiparton processes in hadronic collisions*, *JHEP* **07** (2003) 001, [arXiv:0206293 \[hep-ph\]](#).
32. M. L. Mangano, M. Moretti, and R. Pittau, *Multijet matrix elements and shower evolution in hadronic collisions: $Wb\bar{b} + n$ jets as a case study*, *Nucl. Phys. B* **632** (2002) 343–362, [arXiv:0108069 \[hep-ph\]](#).
33. J. M. Butterworth, J. R. Forshaw, and M. H. Seymour, *Multiparton interactions in photoproduction at HERA*, *Z. Phys.* **C 72** (1996) 637–646, [arXiv:9601371 \[hep-ph\]](#).
34. J. Pumplin et al., *New generation of parton distributions with uncertainties from global QCD analysis*, *JHEP* **07** (2002) 012, [arXiv:0201195 \[hep-ph\]](#).
35. ATLAS Collaboration, *The ATLAS Simulation Infrastructure*, *Eur.Phys.J.* **C70** (2010) 823–874, [arXiv:1005.4568 \[physics.ins-det\]](#).
36. S. Agostinelli et al., *Geant 4 - a simulation toolkit*, *NIM A* **506**, **3** (2003) 250–303.
37. G. Folger and J. P. Wellisch, *String parton models in Geant4*, [arXiv:0306007 \[nucl-th\]](#).
38. H. W. Bertini, *Intranuclear-cascade calculation of the secondary nucleon spectra from nucleon-nucleus interactions in the energy range 340 to 2900 MeV and comparisons with experiment*, *Phys. Rev.* **188** (1969) 1711–1730.
39. ATLAS Collaboration, *Jet energy measurement with the ATLAS detector in proton-proton collisions at $\sqrt{s} = 7$ TeV*, [arXiv:1112.6426 \[hep-ex\]](#).
40. R. Achenbach et al., *The ATLAS Level-1 Calorimeter Trigger*, ATLAS-DAQ-PUB-2008-001. <http://cdsweb.cern.ch/record/1080560>.
41. Atlas Collaboration, *Performance of the ATLAS Trigger System in 2010*, *Eur.Phys.J.* **C72** (2012) 1849, [arXiv:1110.1530 \[hep-ex\]](#).
42. M. Cacciari, G. P. Salam, and G. Soyez, *The anti- k_t jet clustering algorithm*, *JHEP* **04** (2008) 063, [arXiv:0802.1189 \[hep-ph\]](#).
43. M. Cacciari, G. P. Salam, G. Soyez, <http://fastjet.fr/>.
44. W. Lampl et al., *Calorimeter clustering algorithms: description and performance*, ATLAS-LARG-PUB-2008-002. <http://cdsweb.cern.ch/record/1099735>.
45. ATLAS Collaboration, *Expected Performance of the ATLAS Experiment - Detector, Trigger and Physics*, [arXiv:0901.0512 \[hep-ex\]](#).

The ATLAS Collaboration

G. Aad⁴⁷, T. Abajyan²⁰, B. Abbott¹¹⁰, J. Abdallah¹¹, S. Abdel Khalek¹¹⁴, A.A. Abdelalim⁴⁸, O. Abidinov¹⁰, R. Aben¹⁰⁴, B. Abi¹¹¹, M. Abolins⁸⁷, O.S. AbouZeid¹⁵⁷, H. Abramowicz¹⁵², H. Abreu¹³⁵, E. Acerbi^{88a,88b}, B.S. Acharya^{163a,163b}, L. Adamczyk³⁷, D.L. Adams²⁴, T.N. Addy⁵⁵, J. Adelman¹⁷⁵, S. Adomeit⁹⁷, P. Adragna⁷⁴, T. Adye¹²⁸, S. Aefsky²², J.A. Aguilar-Saavedra^{123b,a}, M. Agustoni¹⁶, M. Aharrouche⁸⁰, S.P. Ahlen²¹, F. Ahles⁴⁷, A. Ahmad¹⁴⁷, M. Ahsan⁴⁰, G. Aielli^{132a,132b}, T. Akdogan^{18a}, T.P.A. Åkesson⁷⁸, G. Akimoto¹⁵⁴, A.V. Akimov⁹³, M.S. Alam¹, M.A. Alam⁷⁵, J. Albert¹⁶⁸, S. Albrand⁵⁴, M. Aleksa²⁹, I.N. Aleksandrov⁶³, F. Alessandria^{88a}, C. Alexa^{25a}, G. Alexander¹⁵², G. Alexandre⁴⁸, T. Alexopoulos⁹, M. Alhroob^{163a,163c}, M. Aliev¹⁵, G. Alimonti^{88a}, J. Alison¹¹⁹, B.M.M. Allbrooke¹⁷, P.P. Allport⁷², S.E. Allwood-Spiers⁵², J. Almond⁸¹, A. Aloisio^{101a,101b}, R. Alon¹⁷¹, A. Alonso⁷⁸, F. Alonso⁶⁹, B. Alvarez Gonzalez⁸⁷, M.G. Alviggi^{101a,101b}, K. Amako⁶⁴, C. Amelung²², V.V. Ammosov^{127,*}, A. Amorim^{123a,b}, N. Amram¹⁵², C. Anastopoulos²⁹, L.S. Ancu¹⁶, N. Andari¹¹⁴, T. Andeen³⁴, C.F. Anders^{57b}, G. Anders^{57a}, K.J. Anderson³⁰, A. Andreazza^{88a,88b}, V. Andrei^{57a}, X.S. Anduaga⁶⁹, P. Anger⁴³, A. Angerami³⁴, F. Anghinolfi²⁹, A. Anisenkov¹⁰⁶, N. Anjos^{123a}, A. Annovi⁴⁶, A. Antonaki⁸, M. Antonelli⁴⁶, A. Antonov⁹⁵, J. Antos^{143b}, F. Anulli^{131a}, M. Aoki¹⁰⁰, S. Aoun⁸², L. Aperio Bella⁴, R. Apolle^{117,c}, G. Arabidze⁸⁷, I. Aracena¹⁴², Y. Arai⁶⁴, A.T.H. Arce⁴⁴, S. Arfaoui¹⁴⁷, J-F. Arguin¹⁴, E. Arik^{18a,*}, M. Arik^{18a}, A.J. Armbruster⁸⁶, O. Arnaez⁸⁰, V. Arnal⁷⁹, C. Arnault¹¹⁴, A. Artamonov⁹⁴, G. Artoni^{131a,131b}, D. Arutinov²⁰, S. Asai¹⁵⁴, R. Asfandiyarov¹⁷², S. Ask²⁷, B. Åsman^{145a,145b}, L. Asquith⁵, K. Assamagan²⁴, A. Astbury¹⁶⁸, M. Atkinson¹⁶⁴, B. Aubert⁴, E. Auge¹¹⁴, K. Augsten¹²⁶, M. Auresseau^{144a}, G. Avolio¹⁶², R. Avramidou⁹, D. Axen¹⁶⁷, G. Azuelos^{92,d}, Y. Azuma¹⁵⁴, M.A. Baak²⁹, G. Baccaglioni^{88a}, C. Bacci^{133a,133b}, A.M. Bach¹⁴, H. Bachacou¹³⁵, K. Bachas²⁹, M. Backes⁴⁸, M. Backhaus²⁰, E. Badesco^{25a}, P. Bagnaia^{131a,131b}, S. Bahinipati², Y. Bai^{32a}, D.C. Bailey¹⁵⁷, T. Bain¹⁵⁷, J.T. Baines¹²⁸, O.K. Baker¹⁷⁵, M.D. Baker²⁴, S. Baker⁷⁶, E. Banas³⁸, P. Banerjee⁹², Sw. Banerjee¹⁷², D. Banfi²⁹, A. Bangert¹⁴⁹, V. Bansal¹⁶⁸, H.S. Bansil¹⁷, L. Barak¹⁷¹, S.P. Baranov⁹³, A. Barbaro Galtieri¹⁴, T. Barber⁴⁷, E.L. Barberio⁸⁵, D. Barberis^{49a,49b}, M. Barbero²⁰, D.Y. Bardin⁶³, T. Barillari⁹⁸, M. Barisonzi¹⁷⁴, T. Barklow¹⁴², N. Barlow²⁷, B.M. Barnett¹²⁸, R.M. Barnett¹⁴, A. Baroncelli^{133a}, G. Barone⁴⁸, A.J. Barr¹¹⁷, F. Barreiro⁷⁹, J. Barreiro Guimarães da Costa⁵⁶, P. Barrillon¹¹⁴, R. Bartoldus¹⁴², A.E. Barton⁷⁰, V. Bartsch¹⁴⁸, R.L. Bates⁵², L. Batkova^{143a}, J.R. Batley²⁷, A. Battaglia¹⁶, M. Battistin²⁹, F. Bauer¹³⁵, H.S. Bawa^{142,e}, S. Beale⁹⁷, T. Beau⁷⁷, P.H. Beauchemin¹⁶⁰, R. Beccherle^{49a}, P. Bechtel²⁰, H.P. Beck¹⁶, A.K. Becker¹⁷⁴, S. Becker⁹⁷, M. Beckingham¹³⁷, K.H. Becks¹⁷⁴, A.J. Beddall^{18c}, A. Beddall^{18c}, S. Bedikian¹⁷⁵, V.A. Bednyakov⁶³, C.P. Bee⁸², L.J. Beemster¹⁰⁴, M. Begel²⁴, S. Behar Harpaz¹⁵¹, M. Beimforde⁹⁸, C. Belanger-Champagne⁸⁴, P.J. Bell⁴⁸, W.H. Bell⁴⁸, G. Bella¹⁵², L. Bellagamba^{19a}, F. Bellina²⁹, M. Bellomo²⁹, A. Belloni⁵⁶, O. Beloborodova^{106,f}, K. Belotskiy⁹⁵, O. Beltramello²⁹, O. Benary¹⁵², D. Benchekroun^{134a}, K. Bendtz^{145a,145b}, N. Benekos¹⁶⁴, Y. Benhammou¹⁵², E. Benhar Nocchioli⁴⁸, J.A. Benitez Garcia^{158b}, D.P. Benjamin⁴⁴, M. Benoit¹¹⁴, J.R. Bensinger²², K. Benslama¹²⁹, S. Bentvelsen¹⁰⁴, D. Berge²⁹, E. Bergeaas Kuutmann⁴¹, N. Berger⁴, F. Berghaus¹⁶⁸, E. Berglund¹⁰⁴, J. Beringer¹⁴, P. Bernat⁷⁶, R. Bernhard⁴⁷, C. Bernius²⁴, T. Berry⁷⁵, C. Bertella⁸², A. Bertin^{19a,19b}, F. Bertolucci^{121a,121b}, M.I. Besana^{88a,88b}, G.J. Besjes¹⁰³, N. Besson¹³⁵, S. Bethke⁹⁸, W. Bhimji⁴⁵, R.M. Bianchi²⁹, M. Bianco^{71a,71b}, O. Biebel⁹⁷, S.P. Bieniek⁷⁶, K. Bierwagen⁵³, J. Biesiada¹⁴, M. Biglietti^{133a}, H. Bilokon⁴⁶, M. Bindi^{19a,19b}, S. Binet¹¹⁴, A. Bingul^{18c}, C. Bini^{131a,131b}, C. Biscarat¹⁷⁷, U. Bitenc⁴⁷, K.M. Black²¹, R.E. Blair⁵, J.-B. Blanchard¹³⁵, G. Blanchot²⁹, T. Blazek^{143a}, C. Blocker²², J. Blocki³⁸, A. Blondel⁴⁸, W. Blum⁸⁰, U. Blumenschein⁵³, G.J. Bobbink¹⁰⁴, V.B. Bobrovnikov¹⁰⁶, S.S. Bocchetta⁷⁸, A. Bocchi⁴⁴, C.R. Boddy¹¹⁷, M. Boehler⁴⁷, J. Boek¹⁷⁴, N. Boelaert³⁵, J.A. Bogaerts²⁹, A. Bogdanchikov¹⁰⁶, A. Bogouch^{89,*}, C. Bohm^{145a}, J. Bohm¹²⁴, V. Boisvert⁷⁵, T. Bold³⁷, V. Boldea^{25a}, N.M. Bolnet¹³⁵, M. Bomben⁷⁷, M. Bona⁷⁴, M. Boonekamp¹³⁵, C.N. Booth¹³⁸, S. Bordini⁷⁷, C. Borer¹⁶, A. Borisov¹²⁷, G. Borissov⁷⁰, I. Borjanovic^{12a}, M. Borri⁸¹, S. Borroni⁸⁶, V. Bortolotto^{133a,133b}, K. Bos¹⁰⁴, D. Boscherini^{19a}, M. Bosman¹¹, H. Boterenbrood¹⁰⁴, J. Bouchami⁹², J. Boudreau¹²², E.V. Bouhova-Thacker⁷⁰, D. Boumediene³³, C. Bourdarios¹¹⁴, N. Bousson⁸², A. Boveia³⁰, J. Boyd²⁹, I.R. Boyko⁶³, I. Bozovic-Jelisavcic^{12b}, J. Bracinik¹⁷, P. Branchini^{133a}, A. Brandt⁷, G. Brandt¹¹⁷, O. Brandt⁵³, U. Bratzler¹⁵⁵, B. Brau⁸³, J.E. Brau¹¹³, H.M. Braun^{174,*}, S.F. Brazzale^{163a,163c}, B. Brelier¹⁵⁷, J. Bremer²⁹, K. Brendlinger¹¹⁹, R. Brenner¹⁶⁵, S. Bressler¹⁷¹, D. Britton⁵², F.M. Brochu²⁷, I. Brock²⁰, R. Brock⁸⁷, F. Broggi^{88a}, C. Bromberg⁸⁷, J. Bronner⁹⁸, G. Brooijmans³⁴, T. Brooks⁷⁵, W.K. Brooks^{31b}, G. Brown⁸¹, H. Brown⁷, P.A. Bruckman de Renstrom³⁸, D. Bruncko^{143b}, R. Brunelieire⁴⁷, S. Brunet⁵⁹, A. Bruni^{19a}, G. Bruni^{19a}, M. Bruschi^{19a}, T. Buanes¹³, Q. Buat⁵⁴, F. Bucci⁴⁸, J. Buchanan¹¹⁷, P. Buchholz¹⁴⁰, R.M. Buckingham¹¹⁷, A.G. Buckley⁴⁵, S.I. Buda^{25a}, I.A. Budagov⁶³, B. Budick¹⁰⁷, V. Büscher⁸⁰, L. Bugge¹¹⁶, O. Bulekov⁹⁵, A.C. Bundock⁷², M. Bunse⁴², T. Buran¹¹⁶, H. Burckhart²⁹, S. Burdin⁷², T. Burgess¹³, S. Burke¹²⁸, E. Busato³³, P. Bussey⁵², C.P. Buszello¹⁶⁵, B. Butler¹⁴², J.M. Butler²¹, C.M. Buttar⁵², J.M. Butterworth⁷⁶, W. Buttinger²⁷, S. Cabrera Urbán¹⁶⁶, D. Caforio^{19a,19b}, O. Cakir^{3a}, P. Calafiura¹⁴, G. Calderini⁷⁷, P. Calfayan⁹⁷, R. Calkins¹⁰⁵, L.P. Caloba^{23a}, R. Caloi^{131a,131b}, D. Calvet³³, S. Calvet³³, R. Camacho Toro³³, P. Camarri^{132a,132b}, D. Cameron¹¹⁶, L.M. Caminada¹⁴, S. Campana²⁹, M. Campanelli⁷⁶, V. Canale^{101a,101b}, F. Canelli^{30,g}, A. Canepa^{158a}, J. Cantero⁷⁹, R. Cantrill⁷⁵, L. Capasso^{101a,101b}, M.D.M. Capeans Garrido²⁹, I. Caprini^{25a}, M. Caprini^{25a}, D. Capriotti⁹⁸, M. Capua^{36a,36b}, R. Caputo⁸⁰, R. Cardarelli^{132a}, T. Carli²⁹, G. Carlino^{101a}, L. Carminati^{88a,88b}, B. Caron⁸⁴, S. Caron¹⁰³, E. Carquin^{31b}, G.D. Carrillo Montoya¹⁷², A.A. Carter⁷⁴, J.R. Carter²⁷, J. Carvalho^{123a,h}, D. Casadei¹⁰⁷, M.P. Casado¹¹, M. Cascella^{121a,121b}, C. Caso^{49a,49b,*}, A.M. Castaneda Hernandez^{172,i}, E. Castaneda-Miranda¹⁷², V. Castillo Gimenez¹⁶⁶, N.F. Castro^{123a}, G. Cataldi^{71a}, P. Catastini⁵⁶, A. Catinaccio²⁹, J.R. Catmore²⁹, A. Cattai²⁹, G. Cattani^{132a,132b}, S. Caughron⁸⁷, V. Cavaliere¹⁶⁴, P. Cavalleri⁷⁷, D. Cavalli^{88a}, M. Cavalli-Sforza¹¹, V. Cavasinni^{121a,121b}, F. Ceradini^{133a,133b}, A.S. Cerqueira^{23b}, A. Cerri²⁹, L. Cerrito⁷⁴, F. Cerutti⁴⁶, S.A. Cetin^{18b}, A. Chafaq^{134a}, D. Chakraborty¹⁰⁵, I. Chalupkova¹²⁵, K. Chan², B. Chapleau⁸⁴,

J.D. Chapman²⁷, J.W. Chapman⁸⁶, E. Chareyre⁷⁷, D.G. Charlton¹⁷, V. Chavda⁸¹, C.A. Chavez Barajas²⁹, S. Cheatham⁸⁴, S. Chekanov⁵, S.V. Chekulaev^{158a}, G.A. Chelkov⁶³, M.A. Chelstowska¹⁰³, C. Chen⁶², H. Chen²⁴, S. Chen^{32c}, X. Chen¹⁷², Y. Chen³⁴, A. Cheplakov⁶³, R. Cherkaoui El Moursli^{134e}, V. Chernyatin²⁴, E. Cheu⁶, S.L. Cheung¹⁵⁷, L. Chevalier¹³⁵, G. Chiefari^{101a,101b}, L. Chikovani^{50a,*}, J.T. Childers²⁹, A. Chilingarov⁷⁰, G. Chiodini^{71a}, A.S. Chisholm¹⁷, R.T. Chislett⁷⁶, A. Chitan^{25a}, M.V. Chizhov⁶³, G. Choudalakis³⁰, S. Chouridou¹³⁶, I.A. Christidi⁷⁶, A. Christov⁴⁷, D. Chromek-Burckhart²⁹, M.L. Chu¹⁵⁰, J. Chudoba¹²⁴, G. Ciapetti^{131a,131b}, A.K. Ciftci^{3a}, R. Ciftci^{3a}, D. Cinca³³, V. Cindro⁷³, C. Ciocca^{19a,19b}, A. Ciocio¹⁴, M. Cirilli⁸⁶, P. Cirkovic^{12b}, M. Citterio^{88a}, M. Ciubancan^{25a}, A. Clark⁴⁸, P.J. Clark⁴⁵, R.N. Clarke¹⁴, W. Cleland¹²², J.C. Clemens⁸², B. Clement⁵⁴, C. Clement^{145a,145b}, Y. Coadou⁸², M. Cobal^{163a,163c}, A. Coccaro¹³⁷, J. Cochran⁶², J.G. Cogan¹⁴², J. Coggeshall¹⁶⁴, E. Cogneras¹⁷⁷, J. Colas⁴, S. Cole¹⁰⁵, A.P. Colijn¹⁰⁴, N.J. Collins¹⁷, C. Collins-Tooth⁵², J. Collot⁵⁴, T. Colombo^{118a,118b}, G. Colon⁸³, P. Conde Muno^{123a}, E. Coniavitis¹¹⁷, M.C. Conidi¹¹, S.M. Consonni^{88a,88b}, V. Consorti⁴⁷, S. Constantinescu^{25a}, C. Conta^{118a,118b}, G. Conti⁵⁶, F. Conventi^{101a,j}, M. Cooke¹⁴, B.D. Cooper⁷⁶, A.M. Cooper-Sarkar¹¹⁷, K. Copic¹⁴, T. Cornelissen¹⁷⁴, M. Corradi^{19a}, F. Corriveau^{84,k}, A. Cortes-Gonzalez¹⁶⁴, G. Cortiana⁹⁸, G. Costa^{88a}, M.J. Costa¹⁶⁶, D. Costanzo¹³⁸, T. Costin³⁰, D. Ct²⁹, L. Courneyea¹⁶⁸, G. Cowan⁷⁵, C. Cowden²⁷, B.E. Cox⁸¹, K. Cranmer¹⁰⁷, F. Crescioli^{121a,121b}, M. Cristinziani²⁰, G. Crosetti^{36a,36b}, S. Crp-Renaudin⁵⁴, C.-M. Cuciuc^{25a}, C. Cuenca Almenar¹⁷⁵, T. Cuhadar Donszelmann¹³⁸, M. Curatolo⁴⁶, C.J. Curtis¹⁷, C. Cuthbert¹⁴⁹, P. Cwetanski⁵⁹, H. Czirm¹⁴⁰, P. Czodrowski⁴³, Z. Czczula¹⁷⁵, S. D'Auria⁵², M. D'Onofrio⁷², A. D'Orazio^{131a,131b}, M.J. Da Cunha Sargedas De Sousa^{123a}, C. Da Via⁸¹, W. Dabrowski³⁷, A. Dafinca¹¹⁷, T. Dai⁸⁶, C. Dallapiccola⁸³, M. Dam³⁵, M. Dameri^{49a,49b}, D.S. Damiani¹³⁶, H.O. Danielsson²⁹, V. Dao⁴⁸, G. Darbo^{49a}, G.L. Darlea^{25b}, J.A. Dassoulas⁴¹, W. Davey²⁰, T. Davidek¹²⁵, N. Davidson⁸⁵, R. Davidson⁷⁰, E. Davies^{117,c}, M. Davies⁹², O. Davignon⁷⁷, A.R. Davison⁷⁶, Y. Davygora^{57a}, E. Dawe¹⁴¹, I. Dawson¹³⁸, R.K. Daya-Ishmukhametova²², K. De⁷, R. de Asmundis^{101a}, S. De Castro^{19a,19b}, S. De Cecco⁷⁷, J. de Graat⁹⁷, N. De Groot¹⁰³, P. de Jong¹⁰⁴, C. De La Taille¹¹⁴, H. De la Torre⁷⁹, F. De Lorenzi⁶², L. de Mora⁷⁰, L. De Noij¹⁰⁴, D. De Pedis^{131a}, A. De Salvo^{131a}, U. De Santis^{163a,163c}, A. De Santo¹⁴⁸, J.B. De Vivie De Regie¹¹⁴, G. De Zorzi^{131a,131b}, W.J. Dearnaley⁷⁰, R. Debbe²⁴, C. Debenedetti⁴⁵, B. Dechenaux⁵⁴, D.V. Dedovich⁶³, J. Degenhardt¹¹⁹, C. Del Papa^{163a,163c}, J. Del Peso⁷⁹, T. Del Prete^{121a,121b}, T. Delemontex⁵⁴, M. Deliyergiyev⁷³, A. Dell'Acqua²⁹, L. Dell'Asta²¹, M. Della Pietra^{101a,j}, D. della Volpe^{101a,101b}, M. Delmastro⁴, P.A. Delsart⁵⁴, C. Deluca¹⁰⁴, S. Demers¹⁷⁵, M. Demichev⁶³, B. Demirkoz^{11,l}, J. Deng¹⁶², S.P. Denisov¹²⁷, D. Derendarz³⁸, J.E. Derkaoui^{134d}, F. Derue⁷⁷, P. Dervan⁷², K. Desch²⁰, E. Devetak¹⁴⁷, P.O. Deviveiros¹⁰⁴, A. Dewhurst¹²⁸, B. DeWilde¹⁴⁷, S. Dhaliwal¹⁵⁷, R. Dhullipudi^{24,m}, A. Di Ciaccio^{132a,132b}, L. Di Ciaccio⁴, A. Di Girolamo²⁹, B. Di Girolamo²⁹, S. Di Luise^{133a,133b}, A. Di Mattia¹⁷², B. Di Micco²⁹, R. Di Nardo⁴⁶, A. Di Simone^{132a,132b}, R. Di Sipio^{19a,19b}, M.A. Diaz^{31a}, E.B. Diehl⁸⁶, J. Dietrich⁴¹, T.A. Dietzsch^{57a}, S. Diglio⁸⁵, K. Dindar Yagci³⁹, J. Dingfelder²⁰, F. Dinut^{25a}, C. Dionisi^{131a,131b}, P. Dita^{25a}, S. Dita^{25a}, F. Dittus²⁹, F. Djama⁸², T. Djobava^{50b}, M.A.B. do Vale^{23c}, A. Do Valle Wemans^{123a,n}, T.K.O. Doan⁴, M. Dobbs⁸⁴, R. Dobinson^{29,*}, D. Dobos²⁹, E. Dobson^{29,o}, J. Dodd³⁴, C. Doglioni⁴⁸, T. Doherty⁵², Y. Doi^{64,*}, J. Dolejsi¹²⁵, I. Dolenc⁷³, Z. Dolezal¹²⁵, B.A. Dolgoshein^{95,*}, T. Dohmae¹⁵⁴, M. Donadelli^{23d}, J. Donini³³, J. Dopke²⁹, A. Doria^{101a}, A. Dos Anjos¹⁷², A. Dotti^{121a,121b}, M.T. Dova⁶⁹, A.D. Doxiadis¹⁰⁴, A.T. Doyle⁵², M. Dris⁹, J. Dubbert⁹⁸, S. Dube¹⁴, E. Duchovni¹⁷¹, G. Duckeck⁹⁷, A. Dudarev²⁹, F. Dudziak⁶², M. Dhrssen²⁹, I.P. Duerdoth⁸¹, L. Dufflot¹¹⁴, M.-A. Dufour⁸⁴, L. Duguid⁷⁵, M. Dunford²⁹, H. Duran Yildiz^{3a}, R. Duxfield¹³⁸, M. Dwuznik³⁷, F. Dydak²⁹, M. Dren⁵¹, J. Ebke⁹⁷, S. Eckweiler⁸⁰, K. Edmonds⁸⁰, W. Edson¹, C.A. Edwards⁷⁵, N.C. Edwards⁷⁵, W. Ehrenfeld⁴¹, T. Eifert¹⁴², G. Eigen¹³, K. Einsweiler¹⁴, E. Eisenhandler⁷⁴, T. Ekelof¹⁶⁵, M. El Kacimi^{134c}, M. Ellert¹⁶⁵, S. Elles⁴, F. Ellinghaus⁸⁰, K. Ellis⁷⁴, N. Ellis²⁹, J. Elmsheuser⁹⁷, M. Elsing²⁹, D. Emeliyanov¹²⁸, R. Engelmann¹⁴⁷, A. Engl⁹⁷, B. Epp⁶⁰, J. Erdmann⁵³, A. Ereditato¹⁶, D. Eriksson^{145a}, J. Ernst¹, M. Ernst²⁴, J. Ernwein¹³⁵, D. Errede¹⁶⁴, S. Errede¹⁶⁴, E. Ertel⁸⁰, M. Escalier¹¹⁴, H. Esch⁴², C. Escobar¹²², X. Espinal Curull¹¹, B. Esposito⁴⁶, F. Etienne⁸², A.I. Etiennev¹³⁵, E. Etzion¹⁵², D. Evangelakou⁵³, H. Evans⁵⁹, L. Fabbri^{19a,19b}, C. Fabre²⁹, R.M. Fakhruddinov¹²⁷, S. Falciano^{131a}, Y. Fang¹⁷², M. Fanti^{88a,88b}, A. Farbin⁷, A. Farilla^{133a}, J. Farley¹⁴⁷, T. Farooque¹⁵⁷, S. Farrell¹⁶², S.M. Farrington¹⁶⁹, P. Farthouat²⁹, P. Fassnacht²⁹, D. Fassouliotis⁸, B. Fatholahzadeh¹⁵⁷, A. Favareto^{88a,88b}, L. Fayard¹¹⁴, S. Fazio^{36a,36b}, R. Febbraro³³, P. Federic^{143a}, O.L. Fedin¹²⁰, W. Fedorko⁸⁷, M. Fehling-Kaschek⁴⁷, L. Feligioni⁸², D. Fellmann⁵, C. Feng^{32d}, E.J. Feng⁵, A.B. Fenyuk¹²⁷, J. Ferencei^{143b}, W. Fernando⁵, S. Ferrag⁵², J. Ferrando⁵², V. Ferrara⁴¹, A. Ferrari¹⁶⁵, P. Ferrari¹⁰⁴, R. Ferrari^{118a}, D.E. Ferreira de Lima⁵², A. Ferrer¹⁶⁶, D. Ferrere⁴⁸, C. Ferretti⁸⁶, A. Ferretto Parodi^{49a,49b}, M. Fiascaris³⁰, F. Fiedler⁸⁰, A. Filipi⁷³, F. Filthaut¹⁰³, M. Fincke-Keeler¹⁶⁸, M.C.N. Fiolhais^{123a,h}, L. Fiorini¹⁶⁶, A. Firan³⁹, G. Fischer⁴¹, M.J. Fisher¹⁰⁸, M. Flechl⁴⁷, I. Fleck¹⁴⁰, J. Fleckner⁸⁰, P. Fleischmann¹⁷³, S. Fleischmann¹⁷⁴, T. Flick¹⁷⁴, A. Floderus⁷⁸, L.R. Flores Castillo¹⁷², M.J. Flowerdew⁹⁸, T. Fonseca Martin¹⁶, A. Formica¹³⁵, A. Forti⁸¹, D. Fortin^{158a}, D. Fournier¹¹⁴, H. Fox⁷⁰, P. Francavilla¹¹, M. Franchini^{19a,19b}, S. Franchino^{118a,118b}, D. Francis²⁹, T. Frank¹⁷¹, S. Franz²⁹, M. Fraternali^{118a,118b}, S. Fratina¹¹⁹, S.T. French²⁷, C. Friedrich⁴¹, F. Friedrich⁴³, R. Froeschl²⁹, D. Froidevaux²⁹, J.A. Frost²⁷, C. Fukunaga¹⁵⁵, E. Fullana Torregrosa²⁹, B.G. Fulsom¹⁴², J. Fuster¹⁶⁶, C. Gabaldon²⁹, O. Gabizon¹⁷¹, T. Gadfort²⁴, S. Gadomski⁴⁸, G. Gagliardi^{49a,49b}, P. Gagnon⁵⁹, C. Galea⁹⁷, E.J. Gallas¹¹⁷, V. Gallo¹⁶, B.J. Gallop¹²⁸, P. Gallus¹²⁴, K.K. Gan¹⁰⁸, Y.S. Gao^{142,e}, A. Gaponenko¹⁴, F. Garbersson¹⁷⁵, M. Garcia-Sciveres¹⁴, C. Garca¹⁶⁶, J.E. Garca Navarro¹⁶⁶, R.W. Gardner³⁰, N. Garelli²⁹, H. Garitaonandia¹⁰⁴, V. Garonne²⁹, C. Gatti⁴⁶, G. Gaudio^{118a}, B. Gaur¹⁴⁰, L. Gauthier¹³⁵, P. Gauzzi^{131a,131b}, I.L. Gavrilenko⁹³, C. Gay¹⁶⁷, G. Gaycken²⁰, E.N. Gazis⁹, P. Ge^{32d}, Z. Gece¹⁶⁷, C.N.P. Gee¹²⁸, D.A.A. Geerts¹⁰⁴, Ch. Geich-Gimbel²⁰, K. Gellerstedt^{145a,145b}, C. Gemme^{49a}, A. Gemmell⁵², M.H. Genest⁵⁴, S. Gentile^{131a,131b}, M. George⁵³, S. George⁷⁵, P. Gerlach¹⁷⁴, A. Gershon¹⁵², C. Geweniger^{57a}, H. Ghazlane^{134b}, N. Ghodbane³³, B. Giacobbe^{19a}, S. Giagu^{131a,131b}, V. Giakoumopoulou⁸, V. Giangiobbe¹¹, F. Gianotti²⁹, B. Gibbard²⁴, A. Gibson¹⁵⁷, S.M. Gibson²⁹, D. Gillberg²⁸,

A.R. Gillman¹²⁸, D.M. Gingrich^{2,d}, J. Ginzburg¹⁵², N. Giokaris⁸, M.P. Giordani^{163c}, R. Giordano^{101a,101b}, F.M. Giorgi¹⁵, P. Giovannini⁹⁸, P.F. Giraud¹³⁵, D. Giugni^{88a}, M. Giunta⁹², P. Giusti^{19a}, B.K. Gjelsten¹¹⁶, L.K. Gladilin⁹⁶, C. Glasman⁷⁹, J. Glatzer⁴⁷, A. Glazov⁴¹, K.W. Glitza¹⁷⁴, G.L. Glonti⁶³, J.R. Goddard⁷⁴, J. Godfrey¹⁴¹, J. Godlewski²⁹, M. Goebel⁴¹, T. Göpfert⁴³, C. Goeringer⁸⁰, C. Gössling⁴², S. Goldfarb⁸⁶, T. Golling¹⁷⁵, A. Gomes^{123a,b}, L.S. Gomez Fajardo⁴¹, R. Gonçalves⁷⁵, J. Goncalves Pinto Firmino Da Costa⁴¹, L. Gonella²⁰, S. Gonzalez¹⁷², S. González de la Hoz¹⁶⁶, G. Gonzalez Parra¹¹, M.L. Gonzalez Silva²⁶, S. Gonzalez-Sevilla⁴⁸, J.J. Goodson¹⁴⁷, L. Goossens²⁹, P.A. Gorbounov⁹⁴, H.A. Gordon²⁴, I. Gorelov¹⁰², G. Gorfine¹⁷⁴, B. Gorini²⁹, E. Gorini^{71a,71b}, A. Gorišek⁷³, E. Gornicki³⁸, B. Gosdzik⁴¹, A.T. Goshaw⁵, M. Gosselink¹⁰⁴, M.I. Gostkin⁶³, I. Gough Eschrich¹⁶², M. Gouighri^{134a}, D. Goujdami^{134c}, M.P. Goulette⁴⁸, A.G. Goussiou¹³⁷, C. Goy⁴, S. Gozpinar²², I. Grabowska-Bold³⁷, P. Grafström^{19a,19b}, K.-J. Grah⁴¹, F. Grancagnolo^{71a}, S. Grancagnolo¹⁵, V. Grassi¹⁴⁷, V. Gratchev¹²⁰, N. Grau³⁴, H.M. Gray²⁹, J.A. Gray¹⁴⁷, E. Graziani^{133a}, O.G. Grebenyuk¹²⁰, T. Greenshaw⁷², Z.D. Greenwood^{24,m}, K. Gregersen³⁵, I.M. Gregor⁴¹, P. Grenier¹⁴², J. Griffiths⁷, N. Grigalashvili⁶³, A.A. Grillo¹³⁶, S. Grinstein¹¹, Y.V. Grishkevich⁹⁶, J.-F. Grivaz¹¹⁴, E. Gross¹⁷¹, J. Grosse-Knetter⁵³, J. Groth-Jensen¹⁷¹, K. Grybel¹⁴⁰, D. Guest¹⁷⁵, C. Guicheney³³, S. Guindon⁵³, U. Gul⁵², H. Guler^{84,p}, J. Gunther¹²⁴, B. Guo¹⁵⁷, J. Guo³⁴, P. Gutierrez¹¹⁰, N. Guttman¹⁵², O. Gutzwiller¹⁷², C. Guyot¹³⁵, C. Gwenlan¹¹⁷, C.B. Gwilliam⁷², A. Haas¹⁴², S. Haas²⁹, C. Haber¹⁴, H.K. Hadavand³⁹, D.R. Hadley¹⁷, P. Haefner²⁰, F. Hahn²⁹, S. Haider²⁹, Z. Hajduk³⁸, H. Hakobyan¹⁷⁶, D. Hall¹¹⁷, J. Haller⁵³, K. Hamacher¹⁷⁴, P. Hamal¹¹², M. Hamer⁵³, A. Hamilton^{144b,q}, S. Hamilton¹⁶⁰, L. Han^{32b}, K. Hanagaki¹¹⁵, K. Hanawa¹⁵⁹, M. Hance¹⁴, C. Handel⁸⁰, P. Hanke^{57a}, J.R. Hansen³⁵, J.B. Hansen³⁵, J.D. Hansen³⁵, P.H. Hansen³⁵, P. Hansson¹⁴², K. Hara¹⁵⁹, G.A. Hare¹³⁶, T. Harenberg¹⁷⁴, S. Harkusha⁸⁹, D. Harper⁸⁶, R.D. Harrington⁴⁵, O.M. Harris¹³⁷, J. Hartert⁴⁷, F. Hartjes¹⁰⁴, T. Haruyama⁶⁴, A. Harvey⁵⁵, S. Hasegawa¹⁰⁰, Y. Hasegawa¹³⁹, S. Hassani¹³⁵, S. Haug¹⁶, M. Hauschild²⁹, R. Hauser⁸⁷, M. Havranek²⁰, C.M. Hawkes¹⁷, R.J. Hawkins²⁹, A.D. Hawkins⁷⁸, D. Hawkins¹⁶², T. Hayakawa⁶⁵, T. Hayashi¹⁵⁹, D. Hayden⁷⁵, C.P. Hays¹¹⁷, H.S. Hayward⁷², S.J. Haywood¹²⁸, M. He^{32d}, S.J. Head¹⁷, V. Hedberg⁷⁸, L. Heelan⁷, S. Heim⁸⁷, B. Heinemann¹⁴, S. Heisterkamp³⁵, L. Helary²¹, C. Heller⁹⁷, M. Heller²⁹, S. Hellman^{145a,145b}, D. Hellmich²⁰, C. Helsen¹¹, R.C.W. Henderson⁷⁰, M. Henke^{57a}, A. Henrichs⁵³, A.M. Henriques Correia²⁹, S. Henrot-Versille¹¹⁴, C. Hensei⁵³, T. Henß¹⁷⁴, C.M. Hernandez⁷, Y. Hernández Jiménez¹⁶⁶, R. Herrberg¹⁵, G. Herten⁴⁷, R. Hertenberger⁹⁷, L. Hervas²⁹, G.G. Hesketh⁷⁶, N.P. Hessey¹⁰⁴, E. Higón-Rodríguez¹⁶⁶, J.C. Hill²⁷, K.H. Hiller⁴¹, S. Hillert²⁰, S.J. Hillier¹⁷, I. Hinchliffe¹⁴, E. Hines¹¹⁹, M. Hirose¹¹⁵, F. Hirsch⁴², D. Hirschbuehl¹⁷⁴, J. Hobbs¹⁴⁷, N. Hod¹⁵², M.C. Hodgkinson¹³⁸, P. Hodgson¹³⁸, A. Hoecker²⁹, M.R. Hoferkamp¹⁰², J. Hoffman³⁹, D. Hoffmann⁸², M. Hohlfeld⁸⁰, M. Holder¹⁴⁰, S.O. Holmgren^{145a}, T. Holy¹²⁶, J.L. Holzbauer⁸⁷, T.M. Hong¹¹⁹, L. Hooft van Huysduynen¹⁰⁷, C. Horn¹⁴², S. Horner⁴⁷, J.-Y. Hostachy⁵⁴, S. Hou¹⁵⁰, A. Hoummada^{134a}, J. Howard¹¹⁷, J. Howarth⁸¹, I. Hristova¹⁵, J. Hrivnac¹¹⁴, T. Hryn'ova⁴, P.J. Hsu⁸⁰, S.-C. Hsu¹⁴, Z. Hubacek¹²⁶, F. Hubaut⁸², F. Huegging²⁰, A. Huettmann⁴¹, T.B. Huffman¹¹⁷, E.W. Hughes³⁴, G. Hughes⁷⁰, M. Huhtinen²⁹, M. Hurwitz¹⁴, U. Husemann⁴¹, N. Huseynov^{63,r}, J. Huston⁸⁷, J. Huth⁵⁶, G. Iacobucci⁴⁸, G. Iakovidis⁹, M. Ibbotson⁸¹, I. Ibragimov¹⁴⁰, L. Iconomidou-Fayard¹¹⁴, J. Idarraga¹¹⁴, P. Iengo^{101a}, O. Igonkina¹⁰⁴, Y. Ikegami⁶⁴, M. Ikeno⁶⁴, D. Iliadis¹⁵³, N. Ilic¹⁵⁷, T. Ince²⁰, J. Inigo-Golfín²⁹, P. Ioannou⁸, M. Iodice^{133a}, K. Iordanidou⁸, V. Ippolito^{131a,131b}, A. Irles Quiles¹⁶⁶, C. Isaksson¹⁶⁵, M. Ishino⁶⁶, M. Ishitsuka¹⁵⁶, R. Ishmukhametov³⁹, C. Issever¹¹⁷, S. Istin^{18a}, A.V. Ivashin¹²⁷, W. Iwanski³⁸, H. Iwasaki⁶⁴, J.M. Izen⁴⁰, V. Izzo^{101a}, B. Jackson¹¹⁹, J.N. Jackson⁷², P. Jackson¹⁴², M.R. Jaekel²⁹, V. Jain⁵⁹, K. Jakobs⁴⁷, S. Jakobsen³⁵, T. Jakoubek¹²⁴, J. Jakubek¹²⁶, D.K. Jana¹¹⁰, E. Jansen⁷⁶, H. Jansen²⁹, A. Jantsch⁹⁸, M. Janus⁴⁷, G. Jarlskog⁷⁸, L. Jeanty⁵⁶, I. Jen-La Plante³⁰, D. Jennens⁸⁵, P. Jenni²⁹, A.E. Loevschall-Jensen³⁵, P. Jež³⁵, S. Jézéquel⁴, M.K. Jha^{19a}, H. Ji¹⁷², W. Ji⁸⁰, J. Jia¹⁴⁷, Y. Jiang^{32b}, M. Jimenez Belenguier⁴¹, S. Jin^{32a}, O. Jinnouchi¹⁵⁶, M.D. Joergensen³⁵, D. Joffe³⁹, M. Johansen^{145a,145b}, K.E. Johansson^{145a}, P. Johansson¹³⁸, S. Johnert⁴¹, K.A. Johns⁶, K. Jon-And^{145a,145b}, G. Jones¹⁶⁹, R.W.L. Jones⁷⁰, T.J. Jones⁷², C. Joram²⁹, P.M. Jorge^{123a}, K.D. Joshi⁸¹, J. Jovicevic¹⁴⁶, T. Jovin^{12b}, X. Ju¹⁷², C.A. Jung⁴², R.M. Jungst²⁹, V. Juranek¹²⁴, P. Jussel⁶⁰, A. Juste Rozas¹¹, S. Kabana¹⁶, M. Kaci¹⁶⁶, A. Kaczmarska³⁸, P. Kadlecik³⁵, M. Kado¹¹⁴, H. Kagan¹⁰⁸, M. Kagan⁵⁶, E. Kajomovitz¹⁵¹, S. Kalinin¹⁷⁴, L.V. Kalinovskaya⁶³, S. Kama³⁹, N. Kanaya¹⁵⁴, M. Kaneda²⁹, S. Kaneti²⁷, T. Kanno¹⁵⁶, V.A. Kantserov⁹⁵, J. Kanzaki⁶⁴, B. Kaplan¹⁷⁵, A. Kapliy³⁰, J. Kaplon²⁹, D. Kar⁵², M. Karagounis²⁰, K. Karakostas⁹, M. Karneviskiy⁴¹, V. Kartvelishvili⁷⁰, A.N. Karyukhin¹²⁷, L. Kashi¹⁷², G. Kasieczka^{57b}, R.D. Kass¹⁰⁸, A. Kastanas¹³, M. Kataoka⁴, Y. Kataoka¹⁵⁴, E. Katsoufis⁹, J. Katzy⁴¹, V. Kaushik⁶, K. Kawagoe⁶⁸, T. Kawamoto¹⁵⁴, G. Kawamura⁸⁰, M.S. Kayl¹⁰⁴, S. Kazama¹⁵⁴, V.A. Kazanin¹⁰⁶, M.Y. Kazarinov⁶³, R. Keeler¹⁶⁸, R. Kehoe³⁹, M. Keil⁵³, G.D. Kekelidze⁶³, J.S. Keller¹³⁷, M. Kenyon⁵², O. Kepka¹²⁴, N. Kerschen²⁹, B.P. Kerševan⁷³, S. Kersten¹⁷⁴, K. Kessoku¹⁵⁴, J. Keung¹⁵⁷, F. Khalil-zada¹⁰, H. Khandanyan¹⁶⁴, A. Khanov¹¹¹, D. Kharchenko⁶³, A. Khodinov⁹⁵, A. Khomich^{57a}, T.J. Khoo²⁷, G. Khoraiuli²⁰, A. Khoroshilov¹⁷⁴, V. Khovanskiy⁹⁴, E. Khramov⁶³, J. Khubua^{50b}, H. Kim^{145a,145b}, S.H. Kim¹⁵⁹, N. Kimura¹⁷⁰, O. Kind¹⁵, B.T. King⁷², M. King⁶⁵, R.S.B. King¹¹⁷, J. Kirk¹²⁸, A.E. Kiryunin⁹⁸, T. Kishimoto⁶⁵, D. Kisielewska³⁷, T. Kitamura⁶⁵, T. Kittelmann¹²², E. Kladiva^{143b}, M. Klein⁷², U. Klein⁷², K. Kleinknecht⁸⁰, M. Klemetti⁸⁴, A. Klier¹⁷¹, P. Klimek^{145a,145b}, A. Klimentov²⁴, R. Klingenberg⁴², J.A. Klinger⁸¹, E.B. Klinkby³⁵, T. Kliouchnikova²⁹, P.F. Klok¹⁰³, S. Klous¹⁰⁴, E.-E. Kluge^{57a}, T. Kluge⁷², P. Kluit¹⁰⁴, S. Kluth⁹⁸, N.S. Knecht¹⁵⁷, E. Kneringer⁶⁰, E.B.F.G. Knoops⁸², A. Knue⁵³, B.R. Ko⁴⁴, T. Kobayashi¹⁵⁴, M. Kobel⁴³, M. Kocian¹⁴², P. Kodys¹²⁵, K. Köneke²⁹, A.C. König¹⁰³, S. Koenig⁸⁰, L. Köpke⁸⁰, F. Koetsveld¹⁰³, P. Koevesarki²⁰, T. Koffas²⁸, E. Koffeman¹⁰⁴, L.A. Kogan¹¹⁷, S. Kohlmann¹⁷⁴, F. Kohn⁵³, Z. Kohout¹²⁶, T. Kohriki⁶⁴, T. Koi¹⁴², G.M. Kolachev^{106,*}, H. Kolanoski¹⁵, V. Kolesnikov⁶³, I. Koletsou^{88a}, J. Koll⁸⁷, M. Kollfrath⁴⁷, A.A. Komar⁹³, Y. Komori¹⁵⁴, T. Kondo⁶⁴, T. Kono^{41,s}, A.I. Kononov⁴⁷, R. Konoplich^{107,t}, N. Konstantinidis⁷⁶, S. Koperny³⁷, K. Korczyk³⁸, K. Kordas¹⁵³, A. Korn¹¹⁷, A. Korol¹⁰⁶, I. Korolkov¹¹, E.V. Korolkova¹³⁸, V.A. Korotkov¹²⁷, O. Kortner⁹⁸, S. Kortner⁹⁸, V.V. Kostyukhin²⁰, S. Kotov⁹⁸, V.M. Kotov⁶³, A. Kotwal⁴⁴,

C. Kourkoumelis⁸, V. Kouskoura¹⁵³, A. Koutsman^{158a}, R. Kowalewski¹⁶⁸, T.Z. Kowalski³⁷, W. Kozanecki¹³⁵, A.S. Kozhin¹²⁷, V. Kral¹²⁶, V.A. Kramarenko⁹⁶, G. Kramberger⁷³, M.W. Krasny⁷⁷, A. Krasznahorkay¹⁰⁷, J.K. Kraus²⁰, S. Kreiss¹⁰⁷, F. Krejci¹²⁶, J. Kretschmar⁷², N. Krieger⁵³, P. Krieger¹⁵⁷, K. Kroeninger⁵³, H. Kroha⁹⁸, J. Kroll¹¹⁹, J. Kroseberg²⁰, J. Krstic^{12a}, U. Kruchonak⁶³, H. Krüger²⁰, T. Kruker¹⁶, N. Krumnack⁶², Z.V. Krumshteyn⁶³, T. Kubota⁸⁵, S. Kuday^{3a}, S. Kuehn⁴⁷, A. Kugel^{57c}, T. Kuhl⁴¹, D. Kuhn⁶⁰, V. Kukhtin⁶³, Y. Kulchitsky⁸⁹, S. Kuleshov^{31b}, C. Kummer⁹⁷, M. Kuna⁷⁷, J. Kunkle¹¹⁹, A. Kupco¹²⁴, H. Kurashige⁶⁵, M. Kurata¹⁵⁹, Y.A. Kurochkin⁸⁹, V. Kus¹²⁴, E.S. Kuwertz¹⁴⁶, M. Kuze¹⁵⁶, J. Kvita¹⁴¹, R. Kwee¹⁵, A. La Rosa⁴⁸, L. La Rotonda^{36a,36b}, L. Labarga⁷⁹, J. Labbe⁴, S. Lablak^{134a}, C. Lacasta¹⁶⁶, F. Lacava^{131a,131b}, H. Lacker¹⁵, D. Lacour⁷⁷, V.R. Lacuesta¹⁶⁶, E. Ladygin⁶³, R. Lafaye⁴, B. Laforge⁷⁷, T. Lagouri⁷⁹, S. Lai⁴⁷, E. Laisne⁵⁴, M. Lamanna²⁹, L. Lambourne⁷⁶, C.L. Lampen⁶, W. Lampl⁶, E. Lancon¹³⁵, U. Landgraf⁴⁷, M.P.J. Landon⁷⁴, J.L. Lane⁸¹, V.S. Lang^{57a}, C. Lange⁴¹, A.J. Lankford¹⁶², F. Lanni²⁴, K. Lantzschi¹⁷⁴, S. Laplace⁷⁷, C. Lapoire²⁰, J.F. Laporte¹³⁵, T. Lari^{88a}, A. Larner¹¹⁷, M. Lassnig²⁹, P. Laurelli⁴⁶, V. Lavorini^{36a,36b}, W. Lavrijsen¹⁴, P. Laycock⁷², O. Le Dortz⁷⁷, E. Le Guirriec⁸², C. Le Maner¹⁵⁷, E. Le Menedeu¹¹, T. LeCompte⁵, F. Ledroit-Guillon⁵⁴, H. Lee¹⁰⁴, J.S.H. Lee¹¹⁵, S.C. Lee¹⁵⁰, L. Lee¹⁷⁵, M. Lefebvre¹⁶⁸, M. Legendre¹³⁵, F. Legger⁹⁷, C. Leggett¹⁴, M. Lehmacher²⁰, G. Lehmann Miotto²⁹, X. Lei⁶, M.A.L. Leite^{23d}, R. Leitner¹²⁵, D. Lellouch¹⁷¹, B. Lemmer⁵³, V. Lendermann^{57a}, K.J.C. Leney^{144b}, T. Lenz¹⁰⁴, G. Lenzen¹⁷⁴, B. Lenzi²⁹, K. Leonhardt⁴³, S. Leontsinis⁹, F. Lepold^{57a}, C. Leroy⁹², J-R. Lessard¹⁶⁸, C.G. Lester²⁷, C.M. Lester¹¹⁹, J. Levêque⁴, D. Levin⁸⁶, L.J. Levinson¹⁷¹, A. Lewis¹¹⁷, G.H. Lewis¹⁰⁷, A.M. Leyko²⁰, M. Leyton¹⁵, B. Li⁸², H. Li^{172,u}, S. Li^{32b,v}, X. Li⁸⁶, Z. Liang^{117,w}, H. Liao³³, B. Liberti^{132a}, P. Lichard²⁹, M. Lichtnecker⁹⁷, K. Lie¹⁶⁴, W. Liebzig¹³, C. Limbach²⁰, A. Limosani⁸⁵, M. Limper⁶¹, S.C. Lin^{150,x}, F. Linde¹⁰⁴, J.T. Linnemann⁸⁷, E. Lipeles¹¹⁹, A. Lipniacka¹³, T.M. Liss¹⁶⁴, D. Lissauer²⁴, A. Lister⁴⁸, A.M. Litke¹³⁶, C. Liu²⁸, D. Liu¹⁵⁰, H. Liu⁸⁶, J.B. Liu⁸⁶, L. Liu⁸⁶, M. Liu^{32b}, Y. Liu^{32b}, M. Livan^{118a,118b}, S.S.A. Livermore¹¹⁷, A. Lleres⁵⁴, J. Llorente Merino⁷⁹, S.L. Lloyd⁷⁴, E. Lobodzinska⁴¹, P. Loch⁶, W.S. Lockman¹³⁶, T. Loddenkoetter²⁰, F.K. Loebinger⁸¹, A. Loginov¹⁷⁵, C.W. Loh¹⁶⁷, T. Lohse¹⁵, K. Lohwasser⁴⁷, M. Lokajicek¹²⁴, V.P. Lombardo⁴, R.E. Long⁷⁰, L. Lopes^{123a}, D. Lopez Mateos⁵⁶, J. Lorenz⁹⁷, N. Lorenzo Martinez¹¹⁴, M. Losada¹⁶¹, P. Loscutoff¹⁴, F. Lo Sterzo^{131a,131b}, M.J. Losty^{158a}, X. Lou⁴⁰, A. Lounis¹¹⁴, K.F. Loureiro¹⁶¹, J. Love²¹, P.A. Love⁷⁰, A.J. Lowe^{142,e}, F. Lu^{32a}, H.J. Lubatti¹³⁷, C. Luci^{131a,131b}, A. Lucotte⁵⁴, A. Ludwig⁴³, D. Ludwig⁴¹, I. Ludwig⁴⁷, J. Ludwig⁴⁷, F. Luehring⁵⁹, G. Luijckx¹⁰⁴, W. Lukas⁶⁰, D. Lumb⁴⁷, L. Luminari^{131a}, E. Lund¹¹⁶, B. Lund-Jensen¹⁴⁶, B. Lundberg⁷⁸, J. Lundberg^{145a,145b}, O. Lundberg^{145a,145b}, J. Lundquist³⁵, M. Lungwitz⁸⁰, D. Lynn²⁴, E. Lytken⁷⁸, H. Ma²⁴, L.L. Ma¹⁷², G. Maccarrone⁴⁶, A. Macchiolo⁹⁸, B. Maček⁷³, J. Machado Miguens^{123a}, R. Mackeprang³⁵, R.J. Madaras¹⁴, H.J. Maddocks⁷⁰, W.F. Mader⁴³, R. Maenner^{57c}, T. Maeno²⁴, P. Mättig¹⁷⁴, S. Mättig⁴¹, L. Magnoni²⁹, E. Magradze⁵³, K. Mahboubi⁴⁷, S. Mahmoud⁷², G. Mahout¹⁷, C. Maiani¹³⁵, C. Maidantchik^{23a}, A. Maio^{123a,b}, S. Majewski²⁴, Y. Makida⁶⁴, N. Makovec¹¹⁴, P. Mal¹³⁵, B. Malaescu²⁹, Pa. Malecki³⁸, P. Malecki³⁸, V.P. Maleev¹²⁰, F. Malek⁵⁴, U. Mallik⁶¹, D. Malon⁵, C. Malone¹⁴², S. Maltezos⁹, V. Malyshev¹⁰⁶, S. Malyukov²⁹, R. Mameghani⁹⁷, J. Mamuzic^{12b}, A. Manabe⁶⁴, L. Mandelli^{88a}, I. Mandić⁷³, R. Mandrysch¹⁵, J. Maneira^{123a}, P.S. Mangeard⁸⁷, L. Manhaes de Andrade Filho^{23b}, J.A. Manjarres Ramos¹³⁵, A. Mann⁵³, P.M. Manning¹³⁶, A. Manousakis-Katsikakis⁸, B. Mansoulie¹³⁵, A. Mapelli²⁹, L. Mapelli²⁹, L. March⁷⁹, J.F. Marchand²⁸, F. Marchese^{132a,132b}, G. Marchiori⁷⁷, M. Marcisovsky¹²⁴, C.P. Marino¹⁶⁸, F. Marroquim^{23a}, Z. Marshall²⁹, F.K. Martens¹⁵⁷, L.F. Marti¹⁶, S. Marti-Garcia¹⁶⁶, B. Martin²⁹, B. Martin⁸⁷, J.P. Martin⁹², T.A. Martin¹⁷, V.J. Martin⁴⁵, B. Martin dit Latour⁴⁸, S. Martin-Haugh¹⁴⁸, M. Martinez¹¹, V. Martinez Outschoorn⁵⁶, A.C. Martyniuk¹⁶⁸, M. Marx⁸¹, F. Marzano^{131a}, A. Marzin¹¹⁰, L. Masetti⁸⁰, T. Mashimo¹⁵⁴, R. Mashinistov⁹³, J. Masik⁸¹, A.L. Maslennikov¹⁰⁶, I. Massa^{19a,19b}, G. Massaro¹⁰⁴, N. Massol⁴, P. Mastrandrea¹⁴⁷, A. Mastroberardino^{36a,36b}, T. Masubuchi¹⁵⁴, P. Matricon¹¹⁴, H. Matsunaga¹⁵⁴, T. Matsushita⁶⁵, C. Mattraversi^{117,c}, J. Maurer⁸², S.J. Maxfield⁷², A. Mayne¹³⁸, R. Mazini¹⁵⁰, M. Mazur²⁰, L. Mazzaferro^{132a,132b}, M. Mazzanti^{88a}, S.P. Mc Kee⁸⁶, A. McCarn¹⁶⁴, R.L. McCarthy¹⁴⁷, T.G. McCarthy²⁸, N.A. McCubbin¹²⁸, K.W. McFarlane^{55,*}, J.A. McFayden¹³⁸, G. Mchedlize^{50b}, T. McLaughlan¹⁷, S.J. McMahon¹²⁸, R.A. McPherson^{168,k}, A. Meade⁸³, J. Mechnich¹⁰⁴, M. Mechtel¹⁷⁴, M. Medinnis⁴¹, R. Meera-Lebbai¹¹⁰, T. Meguro¹¹⁵, R. Mehdiyev⁹², S. Mehlhase³⁵, A. Mehta⁷², K. Meier^{57a}, B. Meirose⁷⁸, C. Melachrinos³⁰, B.R. Mellado Garcia¹⁷², F. Meloni^{88a,88b}, L. Mendoza Navas¹⁶¹, Z. Meng^{150,u}, A. Mengarelli^{19a,19b}, S. Menke⁹⁸, E. Meoni¹⁶⁰, K.M. Mercurio⁵⁶, P. Mermod⁴⁸, L. Merola^{101a,101b}, C. Meroni^{88a}, F.S. Merritt³⁰, H. Merritt¹⁰⁸, A. Messina^{29,y}, J. Metcalfe²⁴, A.S. Mete¹⁶², C. Meyer⁸⁰, C. Meyer³⁰, J-P. Meyer¹³⁵, J. Meyer¹⁷³, J. Meyer⁵³, T.C. Meyer²⁹, J. Miao^{32d}, S. Michal²⁹, L. Micu^{25a}, R.P. Middleton¹²⁸, S. Migas⁷², L. Mijovic¹³⁵, G. Mikenberg¹⁷¹, M. Mikestikova¹²⁴, M. Mikuž⁷³, D.W. Miller³⁰, R.J. Miller⁸⁷, W.J. Mills¹⁶⁷, C. Mills⁵⁶, A. Milov¹⁷¹, D.A. Milstead^{145a,145b}, D. Milstein¹⁷¹, A.A. Minaenko¹²⁷, M. Miñano Moya¹⁶⁶, I.A. Minashvili⁶³, A.I. Mincer¹⁰⁷, B. Mindur³⁷, M. Mineev⁶³, Y. Ming¹⁷², L.M. Mir¹¹, G. Mirabelli^{131a}, J. Mitrevski¹³⁶, V.A. Mitsou¹⁶⁶, S. Mitsui⁶⁴, P.S. Miyagawa¹³⁸, J.U. Mjörnmark⁷⁸, T. Moa^{145a,145b}, V. Moeller²⁷, K. Mönig⁴¹, N. Möser²⁰, S. Mohapatra¹⁴⁷, W. Mohr⁴⁷, R. Moles-Valls¹⁶⁶, J. Monk⁷⁶, E. Monnier⁸², J. Montejo Berlingen¹¹, F. Monticelli⁶⁹, S. Monzani^{19a,19b}, R.W. Moore², G.F. Moorhead⁸⁵, C. Mora Herrera⁴⁸, A. Moraes⁵², N. Morange¹³⁵, J. Morel⁵³, G. Morello^{36a,36b}, D. Moreno⁸⁰, M. Moreno Llácer¹⁶⁶, P. Morettini^{49a}, M. Morgenstern⁴³, M. Moroi⁵⁶, A.K. Morley²⁹, G. Mornacchi²⁹, J.D. Morris⁷⁴, L. Morvaj¹⁰⁰, H.G. Moser⁹⁸, M. Mosidze^{50b}, J. Moss¹⁰⁸, R. Mount¹⁴², E. Mountricha^{9,z}, S.V. Mouraviev^{93,*}, E.J.W. Moyse⁸³, F. Mueller^{57a}, J. Mueller¹²², K. Mueller²⁰, T.A. Müller⁹⁷, T. Mueller⁸⁰, D. Muenstermann²⁹, Y. Munwes¹⁵², W.J. Murray¹²⁸, I. Mussche¹⁰⁴, E. Musto^{101a,101b}, A.G. Myagkov¹²⁷, M. Myska¹²⁴, J. Nadal¹¹, K. Nagai¹⁵⁹, R. Nagai¹⁵⁶, K. Nagano⁶⁴, A. Nagarkar¹⁰⁸, Y. Nagasaka⁵⁸, M. Nagel⁹⁸, A.M. Nairz²⁹, Y. Nakahama²⁹, K. Nakamura¹⁵⁴, T. Nakamura¹⁵⁴, I. Nakano¹⁰⁹, G. Nanava²⁰, A. Napier¹⁶⁰, R. Narayan^{57b}, M. Nash^{76,c}, T. Nattermann²⁰, T. Naumann⁴¹, G. Navarro¹⁶¹, H.A. Neal⁸⁶, P.Yu. Nechaeva⁹³, T.J. Neep⁸¹, A. Negri^{118a,118b}, G. Negri²⁹, M. Negrini^{19a}, S. Nektarijevic⁴⁸, A. Nelson¹⁶², T.K. Nelson¹⁴², S. Nemecek¹²⁴, P. Nemethy¹⁰⁷,

A.A. Nepomuceno^{23a}, M. Nessi^{29,aa}, M.S. Neubauer¹⁶⁴, M. Neumann¹⁷⁴, A. Neusiedl⁸⁰, R.M. Neves¹⁰⁷, P. Nevski²⁴, P.R. Newman¹⁷, V. Nguyen Thi Hong¹³⁵, R.B. Nickerson¹¹⁷, R. Nicolaidou¹³⁵, B. Nicquevert²⁹, F. Niedercorn¹¹⁴, J. Nielsen¹³⁶, N. Nikiforou³⁴, A. Nikiforov¹⁵, V. Nikolaenko¹²⁷, I. Nikolic-Audit⁷⁷, K. Nikolics⁴⁸, K. Nikolopoulos¹⁷, H. Nilsen⁴⁷, P. Nilsson⁷, Y. Ninomiya¹⁵⁴, A. Nisati^{131a}, R. Nisius⁹⁸, T. Nobe¹⁵⁶, L. Nodulman⁵, M. Nomachi¹¹⁵, I. Nomidis¹⁵³, S. Norberg¹¹⁰, M. Nordberg²⁹, P.R. Norton¹²⁸, J. Novakova¹²⁵, M. Nozaki⁶⁴, L. Nozka¹¹², I.M. Nugent^{158a}, A.-E. Nuncio-Quiroz²⁰, G. Nunes Hanninger⁸⁵, T. Nunnemann⁹⁷, E. Nurse⁷⁶, B.J. O'Brien⁴⁵, S.W. O'Neale^{17,*}, D.C. O'Neill¹⁴¹, V. O'Shea⁵², L.B. Oakes⁹⁷, F.G. Oakham^{28,d}, H. Oberlack⁹⁸, J. Ocariz⁷⁷, A. Ochi⁶⁵, S. Oda⁶⁸, S. Odaka⁶⁴, J. Odier⁸², H. Ogren⁵⁹, A. Oh⁸¹, S.H. Oh⁴⁴, C.C. Ohm²⁹, T. Ohshima¹⁰⁰, H. Okawa²⁴, Y. Okumura³⁰, T. Okuyama¹⁵⁴, A. Olariu^{25a}, A.G. Olchevski⁶³, S.A. Olivares Pino^{31a}, M. Oliveira^{123a,h}, D. Oliveira Damazio²⁴, E. Oliver Garcia¹⁶⁶, D. Olivito¹¹⁹, A. Olszewski³⁸, J. Olszowska³⁸, A. Onofre^{123a,ab}, P.U.E. Onyisi³⁰, C.J. Oram^{158a}, M.J. Oreglia³⁰, Y. Oren¹⁵², D. Orestano^{133a,133b}, N. Orlando^{71a,71b}, I. Orlov¹⁰⁶, C. Oropeza Barrera⁵², R.S. Orr¹⁵⁷, B. Osculati^{49a,49b}, R. Ospanov¹¹⁹, C. Osuna¹¹, G. Otero y Garzon²⁶, J.P. Ottersbach¹⁰⁴, M. Ouchrif^{134d}, E.A. Ouellette¹⁶⁸, F. Ould-Saada¹¹⁶, A. Ouraou¹³⁵, Q. Ouyang^{32a}, A. Ovcharova¹⁴, M. Owen⁸¹, S. Owen¹³⁸, V.E. Ozcan^{18a}, N. Ozturk⁷, A. Pacheco Pages¹¹, C. Padilla Aranda¹¹, S. Pagan Griso¹⁴, E. Paganis¹³⁸, C. Pahl⁹⁸, F. Paige²⁴, P. Pais⁸³, K. Pajchel¹¹⁶, G. Palacino^{158b}, C.P. Palestini⁶, S. Palestini²⁹, D. Pallin³³, A. Palma^{123a}, J.D. Palmer¹⁷, Y.B. Pan¹⁷², E. Panagiotopoulou⁹, P. Pani¹⁰⁴, N. Panikashvili⁸⁶, S. Panitkin²⁴, D. Pantea^{25a}, A. Papadellis^{145a}, Th.D. Papadopoulou⁹, A. Paramonov⁵, D. Paredes Hernandez³³, W. Park^{24,ac}, M.A. Parker²⁷, F. Parodi^{49a,49b}, J.A. Parsons³⁴, U. Parzefall⁴⁷, S. Pashapour⁵³, E. Pasqualucci^{131a}, S. Passaggio^{49a}, A. Passeri^{133a}, F. Pastore^{133a,133b,*}, Fr. Pastore⁷⁵, G. Pásztor^{48,ad}, S. Pataria¹⁷⁴, N. Patel¹⁴⁹, J.R. Pater⁸¹, S. Patricelli^{101a,101b}, T. Pauly²⁹, M. Pecsny^{143a}, S. Pedraza Lopez¹⁶⁶, M.I. Pedraza Morales¹⁷², S.V. Peleganchuk¹⁰⁶, D. Pelikan¹⁶⁵, H. Peng^{32b}, B. Penning³⁰, A. Penson³⁴, J. Penwell⁵⁹, M. Perantoni^{23a}, K. Perez^{34,ae}, T. Perez Cavalcanti⁴¹, E. Perez Codina^{158a}, M.T. Pérez García-Estañ¹⁶⁶, V. Perez Reale³⁴, L. Perini^{88a,88b}, H. Pernegger²⁹, R. Perrino^{71a}, P. Perrodo⁴, V.D. Peshekhonov⁶³, K. Peters²⁹, B.A. Petersen²⁹, J. Petersen²⁹, T.C. Petersen³⁵, E. Petit⁴, A. Petridis¹⁵³, C. Petridou¹⁵³, E. Petrolu^{131a}, F. Petrucci^{133a,133b}, D. Petschall⁴¹, M. Petteni¹⁴¹, R. Pezoa^{31b}, A. Phan⁸⁵, P.W. Phillips¹²⁸, G. Piacquadio²⁹, A. Picazio⁴⁸, E. Piccaro⁷⁴, M. Piccinini^{19a,19b}, S.M. Piec⁴¹, R. Piegai²⁶, D.T. Pignotti¹⁰⁸, J.E. Pilcher³⁰, A.D. Pilkington⁸¹, J. Pina^{123a,b}, M. Pinamonti^{163a,163c}, A. Pinder¹¹⁷, J.L. Pinfold², B. Pinto^{123a}, C. Pizio^{88a,88b}, M. Plamondon¹⁶⁸, M.-A. Pleier²⁴, E. Plotnikova⁶³, A. Poblaguev²⁴, S. Poddar^{57a}, F. Podlyski³³, L. Poggioli¹¹⁴, M. Pohl⁴⁸, G. Polesello^{118a}, A. Policicchio^{36a,36b}, A. Polini^{19a}, J. Poll⁷⁴, V. Polychronakos²⁴, D. Pomeroy²², K. Pommès²⁹, L. Pontecorvo^{131a}, B.G. Pope⁸⁷, G.A. Popeneciu^{25a}, D.S. Popovic^{12a}, A. Poppleton²⁹, X. Portell Bueso²⁹, G.E. Pospelov⁹⁸, S. Pospisil¹²⁶, I.N. Potrap⁹⁸, C.J. Potter¹⁴⁸, C.T. Potter¹¹³, G. Poulard²⁹, J. Poveda⁵⁹, V. Pozdnyakov⁶³, R. Prabhu⁷⁶, P. Pralavorio⁸², A. Pranko¹⁴, S. Prasad²⁹, R. Pravahan²⁴, S. Prell⁶², K. Pretzl¹⁶, D. Price⁵⁹, J. Price⁷², L.E. Price⁵, D. Prieur¹²², M. Primavera^{71a}, K. Prokofiev¹⁰⁷, F. Prokoshin^{31b}, S. Protopopescu²⁴, J. Proudfoot⁵, X. Prudent⁴³, M. Przybycien³⁷, H. Przysiezniak⁴, S. Psoroulas²⁰, E. Ptacek¹¹³, E. Pueschel⁸³, J. Purdham⁸⁶, M. Purohit^{24,ac}, P. Puzo¹¹⁴, Y. Pylypchenko⁶¹, J. Qian⁸⁶, A. Quadt⁵³, D.R. Quarrie¹⁴, W.B. Quayle¹⁷², F. Quinonez^{31a}, M. Raas¹⁰³, V. Radescu⁴¹, P. Radloff¹¹³, T. Rador^{18a}, F. Ragusa^{88a,88b}, G. Rahal¹⁷⁷, A.M. Rahimi¹⁰⁸, D. Rahm²⁴, S. Rajagopalan²⁴, M. Rammensee⁴⁷, M. Rammes¹⁴⁰, A.S. Randle-Conde³⁹, K. Randrianarivony²⁸, F. Rauscher⁹⁷, T.C. Rave⁴⁷, M. Raymond²⁹, A.L. Read¹¹⁶, D.M. Rebuffi^{118a,118b}, A. Redelbach¹⁷³, G. Redlinger²⁴, R. Reece¹¹⁹, K. Reeves⁴⁰, E. Reinherz-Aronis¹⁵², A. Reinsch¹¹³, H. Reisin²⁶, I. Reisinger⁴², C. Rembser²⁹, Z.L. Ren¹⁵⁰, A. Renaud¹¹⁴, M. Rescigno^{131a}, S. Resconi^{88a}, B. Resende¹³⁵, P. Reznicek⁹⁷, R. Rezvani¹⁵⁷, R. Richter⁹⁸, E. Richter-Was^{4,af}, M. Ridel⁷⁷, M. Rijpstra¹⁰⁴, M. Rijssenbeek¹⁴⁷, A. Rimoldi^{118a,118b}, L. Rinaldi^{19a}, R.R. Rios³⁹, I. Riu¹¹, G. Rivoltella^{88a,88b}, F. Rizatdinova¹¹¹, E. Rizvi⁷⁴, S.H. Robertson^{84,k}, A. Robichaud-Veronneau¹¹⁷, D. Robinson²⁷, J.E.M. Robinson⁸¹, A. Robson⁵², J.G. Rocha de Lima¹⁰⁵, C. Roda^{121a,121b}, D. Roda Dos Santos²⁹, A. Roe⁵³, S. Roe²⁹, O. Røhne¹¹⁶, S. Rolli¹⁶⁰, A. Romaniouk⁹⁵, M. Romano^{19a,19b}, G. Romeo²⁶, E. Romero Adam¹⁶⁶, L. Roos⁷⁷, E. Ros¹⁶⁶, S. Rosati^{131a}, K. Rosbach⁴⁸, A. Rose¹⁴⁸, M. Rose⁷⁵, G.A. Rosenbaum¹⁵⁷, E.I. Rosenberg⁶², P.L. Rosendahl¹³, O. Rosenthal¹⁴⁰, L. Rosselet⁴⁸, V. Rossetti¹¹, E. Rossi^{131a,131b}, L.P. Rossi^{49a}, M. Rotaru^{25a}, I. Roth¹⁷¹, J. Rothberg¹³⁷, D. Rousseau¹¹⁴, C.R. Royon¹³⁵, A. Rozanov⁸², Y. Rozen¹⁵¹, X. Ruan^{32a,ag}, F. Rubbo¹¹, I. Rubinskiy⁴¹, N. Ruckstuhl¹⁰⁴, V.I. Rud⁹⁶, C. Rudolph⁴³, G. Rudolph⁶⁰, F. Rühr⁶, A. Ruiz-Martinez⁶², L. Ruyantsev⁶³, Z. Rurikova⁴⁷, N.A. Rusakovich⁶³, J.P. Rutherford⁶, C. Ruwiedel^{14,*}, P. Ruzicka¹²⁴, Y.F. Ryabov¹²⁰, M. Rybar¹²⁵, G. Rybkin¹¹⁴, N.C. Ryder¹¹⁷, A.F. Saavedra¹⁴⁹, S. Sacerdoti²⁶, I. Sadeh¹⁵², H.F.-W. Sadrozinski¹³⁶, R. Sadykov⁶³, F. Safai Tehrani^{131a}, H. Sakamoto¹⁵⁴, G. Salamanna⁷⁴, A. Salamon^{132a}, M. Saleem¹¹⁰, D. Salek²⁹, D. Salihagic⁹⁸, A. Salkov¹⁴², J. Salt¹⁶⁶, B.M. Salvachua Ferrando⁵, D. Salvatore^{36a,36b}, F. Salvatore¹⁴⁸, A. Salvucci¹⁰³, A. Salzburger²⁹, D. Sampsonidis¹⁵³, B.H. Samset¹¹⁶, A. Sanchez^{101a,101b}, V. Sanchez Martinez¹⁶⁶, H. Sandaker¹³, H.G. Sander⁸⁰, M.P. Sanders⁹⁷, M. Sandhoff¹⁷⁴, T. Sandoval²⁷, C. Sandoval¹⁶¹, R. Sandstroem⁹⁸, D.P.C. Sankey¹²⁸, A. Sansoni⁴⁶, C. Santamarina Rios⁸⁴, C. Santoni³³, R. Santonico^{132a,132b}, H. Santos^{123a}, J.G. Saraiva^{123a}, T. Sarangi¹⁷², E. Sarkisyan-Grinbaum⁷, F. Sarri^{121a,121b}, G. Sartisohn¹⁷⁴, O. Sasaki⁶⁴, Y. Sasaki¹⁵⁴, N. Sasao⁶⁶, I. Satsounkevitch⁸⁹, G. Sauvage^{4,*}, E. Sauvan⁴, J.B. Sauvan¹¹⁴, P. Savard^{157,d}, V. Savinov¹²², D.O. Savu²⁹, L. Sawyer^{24,m}, D.H. Saxon⁵², J. Saxon¹¹⁹, C. Sbarra^{19a}, A. Sbrizzi^{19a,19b}, D.A. Scannicchio¹⁶², M. Scarcella¹⁴⁹, J. Schaarschmidt¹¹⁴, P. Schacht⁹⁸, D. Schaefer¹¹⁹, U. Schäfer⁸⁰, S. Schaepe²⁰, S. Schaezel^{57b}, A.C. Schaffer¹¹⁴, D. Schaile⁹⁷, R.D. Schamberger¹⁴⁷, A.G. Schamov¹⁰⁶, V. Scharf^{57a}, V.A. Schegelsky¹²⁰, D. Scheirich⁸⁶, M. Schernau¹⁶², M.I. Scherzer³⁴, C. Schiavi^{49a,49b}, J. Schieck⁹⁷, M. Schioppa^{36a,36b}, S. Schlenker²⁹, E. Schmidt⁴⁷, K. Schmieden²⁰, C. Schmitt⁸⁰, S. Schmitt^{57b}, M. Schmitz²⁰, B. Schneider¹⁶, U. Schnoor⁴³, A. Schoening^{57b}, A.L.S. Schorlemmer⁵³, M. Schott²⁹, D. Schouten^{158a}, J. Schovancova¹²⁴, M. Schram⁸⁴, C. Schroeder⁸⁰, N. Schroer^{57c}, M.J. Schultens²⁰, J. Schultes¹⁷⁴, H.-C. Schultz-Coulon^{57a}, H. Schulz¹⁵,

M. Schumacher⁴⁷, B.A. Schumm¹³⁶, Ph. Schune¹³⁵, C. Schwanenberger⁸¹, A. Schwartzman¹⁴², Ph. Schwemling⁷⁷,
 R. Schwienhorst⁸⁷, R. Schwierz⁴³, J. Schwindling¹³⁵, T. Schwindt²⁰, M. Schwoerer⁴, G. Sciolla²², W.G. Scott¹²⁸, J. Searcy¹¹³,
 G. Sedov⁴¹, E. Sedykh¹²⁰, S.C. Seidel¹⁰², A. Seiden¹³⁶, F. Seifert⁴³, J.M. Seixas^{23a}, G. Sekhniaidze^{101a}, S.J. Sekula³⁹,
 K.E. Selbach⁴⁵, D.M. Seliverstov¹²⁰, B. Sellden^{145a}, G. Sellers⁷², M. Seman^{143b}, N. Semprini-Cesari^{19a,19b}, C. Serfon⁹⁷,
 L. Serin¹¹⁴, L. Serkin⁵³, R. Seuster⁹⁸, H. Severini¹¹⁰, A. Sfyrta²⁹, E. Shabalina⁵³, M. Shamim¹¹³, L.Y. Shan^{32a}, J.T. Shank²¹,
 Q.T. Shao⁸⁵, M. Shapiro¹⁴, P.B. Shatalov⁹⁴, K. Shaw^{163a,163c}, D. Sherman¹⁷⁵, P. Sherwood⁷⁶, A. Shibata¹⁰⁷, S. Shimizu²⁹,
 M. Shimojima⁹⁹, T. Shin⁵⁵, M. Shiyakova⁶³, A. Shmeleva⁹³, M.J. Shochet³⁰, D. Short¹¹⁷, S. Shrestha⁶², E. Shulga⁹⁵,
 M.A. Shupe⁶, P. Sicho¹²⁴, A. Sidoti^{131a}, F. Siegert⁴⁷, Dj. Sijacki^{12a}, O. Silbert¹⁷¹, J. Silva^{123a}, Y. Silver¹⁵², D. Silverstein¹⁴²,
 S.B. Silverstein^{145a}, V. Simak¹²⁶, O. Simard¹³⁵, Lj. Simic^{12a}, S. Simion¹¹⁴, E. Simioni⁸⁰, B. Simmons⁷⁶, R. Simoniello^{88a,88b},
 M. Simonyan³⁵, P. Sinervo¹⁵⁷, N.B. Sinev¹¹³, V. Sipica¹⁴⁰, G. Siragusa¹⁷³, A. Sircar²⁴, A.N. Sisakyan^{63,*}, S.Yu. Sivoklov⁹⁶,
 J. Sjölin^{145a,145b}, T.B. Sjurson¹³, L.A. Skinnari¹⁴, H.P. Skottowe⁵⁶, K. Skovpen¹⁰⁶, P. Skubic¹¹⁰, M. Slater¹⁷, T. Slavicek¹²⁶,
 K. Sliwa¹⁶⁰, V. Smakhtin¹⁷¹, B.H. Smart⁴⁵, S.Yu. Smirnov⁹⁵, Y. Smirnov⁹⁵, L.N. Smirnova⁹⁶, O. Smirnova⁷⁸, B.C. Smith⁵⁶,
 D. Smith¹⁴², K.M. Smith⁵², M. Smizanska⁷⁰, K. Smolek¹²⁶, A.A. Snesarev⁹³, S.W. Snow⁸¹, J. Snow¹¹⁰, S. Snyder²⁴,
 R. Sobie^{168,k}, J. Sodomka¹²⁶, A. Soffer¹⁵², C.A. Solans¹⁶⁶, M. Solar¹²⁶, J. Solc¹²⁶, E.Yu. Soldatov⁹⁵, U. Soldevila¹⁶⁶,
 E. Solfaroli Camillocci^{131a,131b}, A.A. Solodkov¹²⁷, O.V. Solovyanov¹²⁷, V. Solovyev¹²⁰, N. Soni⁸⁵, V. Sopko¹²⁶, B. Sopko¹²⁶,
 M. Sosebee⁷, R. Soualah^{163a,163c}, A. Soukharev¹⁰⁶, S. Spagnolo^{71a,71b}, F. Spano⁷⁵, R. Spighi^{19a}, G. Spigo²⁹, R. Spiwoaks²⁹,
 M. Spousta^{125,ah}, T. Spreitzer¹⁵⁷, B. Spurlock⁷, R.D. St. Denis⁵², J. Stahlman¹¹⁹, R. Stamen^{57a}, E. Stanecka³⁸, R.W. Stanek⁵,
 C. Stanescu^{133a}, M. Stanescu-Bellu⁴¹, S. Stapnes¹¹⁶, E.A. Starchenko¹²⁷, J. Stark⁵⁴, P. Staroba¹²⁴, P. Starovoitov⁴¹,
 R. Staszewski³⁸, A. Staude⁹⁷, P. Stavina^{143a,*}, G. Steele⁵², P. Steinbach⁴³, P. Steinberg²⁴, I. Stekl¹²⁶, B. Stelzer¹⁴¹,
 H.J. Stelzer⁸⁷, O. Stelzer-Chilton^{158a}, H. Stenzel⁵¹, S. Stern⁹⁸, G.A. Stewart²⁹, J.A. Stillings²⁰, M.C. Stockton⁸⁴, K. Stoerig⁴⁷,
 G. Stoicea^{25a}, S. Stonjek⁹⁸, P. Strachota¹²⁵, A.R. Stradling⁷, A. Straessner⁴³, J. Strandberg¹⁴⁶, S. Strandberg^{145a,145b},
 A. Strandlie¹¹⁶, M. Strang¹⁰⁸, E. Strauss¹⁴², M. Strauss¹¹⁰, P. Strizenec^{143b}, R. Ströhmer¹⁷³, D.M. Strom¹¹³, J.A. Strong^{75,*},
 R. Stroynowski³⁹, J. Strube¹²⁸, B. Stugu¹³, I. Stumer^{24,*}, J. Stupak¹⁴⁷, P. Sturm¹⁷⁴, N.A. Styles⁴¹, D.A. Soh^{150,w}, D. Su¹⁴²,
 H.S. Subramania², A. Succurro¹¹, Y. Sugaya¹¹⁵, C. Suhr¹⁰⁵, M. Suk¹²⁵, V.V. Sulimov⁹³, S. Sultansoy^{3d}, T. Sumida⁶⁶, X. Sun⁵⁴,
 J.E. Sundermann⁴⁷, K. Suruliz¹³⁸, G. Susinno^{36a,36b}, M.R. Sutton¹⁴⁸, Y. Suzuki⁶⁴, Y. Suzuki⁶⁵, M. Svatos¹²⁴, S. Swedish¹⁶⁷,
 I. Sykora^{143a}, T. Sykora¹²⁵, J. Sánchez¹⁶⁶, D. Ta¹⁰⁴, K. Tackmann⁴¹, A. Taffard¹⁶², R. Tafirout^{158a}, N. Taiblum¹⁵²,
 Y. Takahashi¹⁰⁰, H. Takai²⁴, R. Takashima⁶⁷, H. Takeda⁶⁵, T. Takeshita¹³⁹, Y. Takubo⁶⁴, M. Talby⁸², A. Talyshv^{106,f},
 M.C. Tamsett²⁴, J. Tanaka¹⁵⁴, R. Tanaka¹¹⁴, S. Tanaka¹³⁰, S. Tanaka⁶⁴, A.J. Tanasijczuk¹⁴¹, K. Tani⁶⁵, N. Tannoury⁸²,
 S. Tapprogge⁸⁰, D. Tardif¹⁵⁷, S. Tarem¹⁵¹, F. Tarrade²⁸, G.F. Tartarelli^{88a}, P. Tas¹²⁵, M. Tasevsky¹²⁴, E. Tassi^{36a,36b},
 M. Tatarikhov¹⁴, Y. Tayalati^{134d}, C. Taylor⁷⁶, F.E. Taylor⁹¹, G.N. Taylor⁸⁵, W. Taylor^{158b}, M. Teinturier¹¹⁴,
 M. Teixeira Dias Castanheira⁷⁴, P. Teixeira-Dias⁷⁵, K.K. Temming⁴⁷, H. Ten Kate²⁹, P.K. Teng¹⁵⁰, S. Terada⁶⁴, K. Terashi¹⁵⁴,
 J. Terron⁷⁹, M. Testa⁴⁶, R.J. Teuscher^{157,k}, J. Therhaag²⁰, T. Theveneaux-Pelzer⁷⁷, S. Thoma⁴⁷, J.P. Thomas¹⁷,
 E.N. Thompson³⁴, P.D. Thompson¹⁷, P.D. Thompson¹⁵⁷, A.S. Thompson⁵², L.A. Thomsen³⁵, E. Thomson¹¹⁹, M. Thomson²⁷,
 W.M. Thong⁸⁵, R.P. Thun⁸⁶, F. Tian³⁴, M.J. Tibbetts¹⁴, T. Tic¹²⁴, V.O. Tikhomirov⁹³, Y.A. Tikhonov^{106,f}, S. Timoshenko⁹⁵,
 P. Tipton¹⁷⁵, S. Tisserant⁸², T. Todorov⁴, S. Todorova-Nova¹⁶⁰, B. Toggerson¹⁶², J. Tojo⁶⁸, S. Tokár^{143a}, K. Tokushuku⁶⁴,
 K. Tollefson⁸⁷, M. Tomoto¹⁰⁰, L. Tompkins³⁰, K. Toms¹⁰², A. Tonoyan¹³, C. Topfel¹⁶, N.D. Topilin⁶³, I. Torchiani²⁹,
 E. Torrence¹¹³, H. Torres⁷⁷, E. Torrón Pastor¹⁶⁶, J. Toth^{82,ad}, F. Touchard⁸², D.R. Tovey¹³⁸, T. Trefzger¹⁷³, L. Tremblet²⁹,
 A. Tricoli²⁹, I.M. Trigger^{158a}, S. Trincz-Duvoid⁷⁷, M.F. Tripiana⁶⁹, N. Triplett²⁴, W. Trischuk¹⁵⁷, B. Trocmé⁵⁴, C. Troncon^{88a},
 M. Trotter-McDonald¹⁴¹, M. Trzebinski³⁸, A. Trzupek³⁸, C. Tsarouchas²⁹, J.C.-L. Tseng¹¹⁷, M. Tsiakiris¹⁰⁴, P.V. Tsiarehshka⁸⁹,
 D. Tsionou^{4,ai}, G. Tsipolitis⁹, S. Tsiskaridze¹¹, V. Tsiskaridze⁴⁷, E.G. Tskhadadze^{50a}, I.I. Tsukerman⁹⁴, V. Tsulaia¹⁴,
 J.-W. Tsung²⁰, S. Tsuno⁶⁴, D. Tsybychev¹⁴⁷, A. Tua¹³⁸, A. Tudorache^{25a}, V. Tudorache^{25a}, J.M. Tuggle³⁰, M. Turala³⁸,
 D. Turecek¹²⁶, I. Turk Cakir^{3e}, E. Turlay¹⁰⁴, R. Turra^{88a,88b}, P.M. Tuts³⁴, A. Tykhonov⁷³, M. Tylmad^{145a,145b}, M. Tyndel¹²⁸,
 G. Tzanakos⁸, K. Uchida²⁰, I. Ueda¹⁵⁴, R. Ueno²⁸, M. Uglund¹³, M. Uhlenbrock²⁰, M. Uhrmacher⁵³, F. Ukegawa¹⁵⁹, G. Unal²⁹,
 A. Undrus²⁴, G. Unel¹⁶², Y. Unno⁶⁴, D. Urbaniec³⁴, G. Usai⁷, M. Uslenghi^{118a,118b}, L. Vacavant⁸², V. Vacek¹²⁶, B. Vachon⁸⁴,
 S. Vahsen¹⁴, J. Valenta¹²⁴, S. Valentini^{19a,19b}, A. Valero¹⁶⁶, S. Valkar¹²⁵, E. Valladolid Gallego¹⁶⁶, S. Vallecorsa¹⁵¹,
 J.A. Valls Ferrer¹⁶⁶, P.C. Van Der Deijl¹⁰⁴, R. van der Geer¹⁰⁴, H. van der Graaf¹⁰⁴, R. Van Der Leeuw¹⁰⁴, E. van der Poel¹⁰⁴,
 D. van der Ster²⁹, N. van Eldik²⁹, P. van Gemmeren⁵, I. van Vulpen¹⁰⁴, M. Vanadia⁹⁸, W. Vandelli²⁹, A. Vaniachine⁵,
 P. Vankov⁴¹, F. Vannucci⁷⁷, R. Vari^{131a}, T. Varol⁸³, D. Varouchas¹⁴, A. Vartapetian⁷, K.E. Varvell¹⁴⁹, V.I. Vassilakopoulos⁵⁵,
 F. Vazeille³³, T. Vazquez Schroeder⁵³, G. Vegni^{88a,88b}, J.J. Veillet¹¹⁴, F. Veloso^{123a}, R. Veness²⁹, S. Veneziano^{131a},
 A. Ventura^{71a,71b}, D. Ventura⁸³, M. Venturi⁴⁷, N. Venturi¹⁵⁷, V. Vercesi^{118a}, M. Verducci¹³⁷, W. Verkerke¹⁰⁴, J.C. Vermeulen¹⁰⁴,
 A. Vest⁴³, M.C. Vetterli^{141,d}, I. Vichou¹⁶⁴, T. Vickey^{144b,aj}, O.E. Vickey Boeriu^{144b}, G.H.A. Viehhauser¹¹⁷, S. Viel¹⁶⁷,
 M. Villa^{19a,19b}, M. Villaplana Perez¹⁶⁶, E. Vilucchi⁴⁶, M.G. Vincet²⁸, E. Vinek²⁹, V.B. Vinogradov⁶³, M. Virchaux^{135,*},
 J. Virzi¹⁴, O. Vitells¹⁷¹, M. Viti⁴¹, I. Vivarelli⁴⁷, F. Vives Vaque², S. Vlachos⁹, D. Vladioiu⁹⁷, M. Vlasak¹²⁶, A. Vogel²⁰,
 P. Vokac¹²⁶, G. Volpi⁴⁶, M. Volpi⁸⁵, G. Volpini^{88a}, H. von der Schmitt⁹⁸, H. von Radziewski⁴⁷, E. von Toerne²⁰, V. Vorobel¹²⁵,
 V. Vorwerk¹¹, M. Vos¹⁶⁶, R. Voss²⁹, T.T. Voss¹⁷⁴, J.H. Vosseveld⁷², N. Vranjes¹³⁵, M. Vranjes Milosavljevic¹⁰⁴, V. Vrba¹²⁴,
 M. Vreeswijk¹⁰⁴, T. Vu Anh⁴⁷, R. Vuillermet²⁹, I. Vukotic³⁰, W. Wagner¹⁷⁴, P. Wagner¹¹⁹, H. Wahlen¹⁷⁴, S. Wahrmund⁴³,
 J. Wakabayashi¹⁰⁰, S. Walch⁸⁶, J. Walder⁷⁰, R. Walker⁹⁷, W. Walkowiak¹⁴⁰, R. Wall¹⁷⁵, P. Waller⁷², B. Walsh¹⁷⁵, C. Wang⁴⁴,
 H. Wang¹⁷², H. Wang^{32b,ak}, J. Wang¹⁵⁰, J. Wang⁵⁴, R. Wang¹⁰², S.M. Wang¹⁵⁰, T. Wang²⁰, A. Warburton⁸⁴, C.P. Ward²⁷,
 M. Warsinsky⁴⁷, A. Washbrook⁴⁵, C. Wasicki⁴¹, I. Watanabe⁶⁵, P.M. Watkins¹⁷, A.T. Watson¹⁷, I.J. Watson¹⁴⁹, M.F. Watson¹⁷,

G. Watts¹³⁷, S. Watts⁸¹, A.T. Waugh¹⁴⁹, B.M. Waugh⁷⁶, M.S. Weber¹⁶, P. Weber⁵³, A.R. Weidberg¹¹⁷, P. Weigell⁹⁸, J. Weingarten⁵³, C. Weiser⁴⁷, H. Wellenstein²², P.S. Wells²⁹, T. Wenaus²⁴, D. Wendland¹⁵, Z. Weng^{150,w}, T. Wengler²⁹, S. Wenig²⁹, N. Wermes²⁰, M. Werner⁴⁷, P. Werner²⁹, M. Werth¹⁶², M. Wessels^{57a}, J. Wetter¹⁶⁰, C. Weydert⁵⁴, K. Whalen²⁸, S.J. Wheeler-Ellis¹⁶², A. White⁷, M.J. White⁸⁵, S. White^{121a,121b}, S.R. Whitehead¹¹⁷, D. Whiteson¹⁶², D. Whittington⁵⁹, F. Wicek¹¹⁴, D. Wicke¹⁷⁴, F.J. Wickens¹²⁸, W. Wiedenmann¹⁷², M. Wielers¹²⁸, P. Wienemann²⁰, C. Wigglesworth⁷⁴, L.A.M. Wiik-Fuchs⁴⁷, P.A. Wijeratne⁷⁶, A. Wildauer⁹⁸, M.A. Wildt^{41,s}, I. Wilhelm¹²⁵, H.G. Wilkens²⁹, J.Z. Will⁹⁷, E. Williams³⁴, H.H. Williams¹¹⁹, W. Willis³⁴, S. Willocq⁸³, J.A. Wilson¹⁷, M.G. Wilson¹⁴², A. Wilson⁸⁶, I. Wingerter-Seez⁴, S. Winkelmann⁴⁷, F. Winklmeier²⁹, M. Wittgen¹⁴², S.J. Wollstadt⁸⁰, M.W. Wolter³⁸, H. Wolters^{123a,h}, W.C. Wong⁴⁰, G. Wooden⁸⁶, B.K. Wosiek³⁸, J. Wotschack²⁹, M.J. Woudstra⁸¹, K.W. Wozniak³⁸, K. Wraight⁵², M. Wright⁵², B. Wrona⁷², S.L. Wu¹⁷², X. Wu⁴⁸, Y. Wu^{32b,al}, E. Wulf³⁴, B.M. Wynne⁴⁵, S. Xella³⁵, M. Xiao¹³⁵, S. Xie⁴⁷, C. Xu^{32b,z}, D. Xu¹³⁸, B. Yabsley¹⁴⁹, S. Yacoob^{144b}, M. Yamada⁶⁴, H. Yamaguchi¹⁵⁴, A. Yamamoto⁶⁴, K. Yamamoto⁶², S. Yamamoto¹⁵⁴, T. Yamamura¹⁵⁴, T. Yamanaka¹⁵⁴, J. Yamaoka⁴⁴, T. Yamazaki¹⁵⁴, Y. Yamazaki⁶⁵, Z. Yan²¹, H. Yang⁸⁶, U.K. Yang⁸¹, Y. Yang⁵⁹, Z. Yang^{145a,145b}, S. Yanush⁹⁰, L. Yao^{32a}, Y. Yao¹⁴, Y. Yasu⁶⁴, G.V. Ybeles Smit¹²⁹, J. Ye³⁹, S. Ye²⁴, M. Yilmaz^{3c}, R. Yoosofmiya¹²², K. Yorita¹⁷⁰, R. Yoshida⁵, C. Young¹⁴², C.J. Young¹¹⁷, S. Youssef²¹, D. Yu²⁴, J. Yu⁷, J. Yu¹¹¹, L. Yuan⁶⁵, A. Yurkewicz¹⁰⁵, M. Byszewski²⁹, B. Zabinski³⁸, R. Zaidan⁶¹, A.M. Zaitsev¹²⁷, Z. Zajacova²⁹, L. Zanello^{131a,131b}, A. Zaytsev¹⁰⁶, C. Zeitnitz¹⁷⁴, M. Zeman¹²⁴, A. Zemla³⁸, C. Zender²⁰, O. Zenin¹²⁷, T. Ženiš^{143a}, Z. Zinonos^{121a,121b}, S. Zenz¹⁴, D. Zerwas¹¹⁴, G. Zevi della Porta⁵⁶, Z. Zhan^{32d}, D. Zhang^{32b,ak}, H. Zhang⁸⁷, J. Zhang⁵, X. Zhang^{32d}, Z. Zhang¹¹⁴, L. Zhao¹⁰⁷, T. Zhao¹³⁷, Z. Zhao^{32b}, A. Zhemchugov⁶³, J. Zhong¹¹⁷, B. Zhou⁸⁶, N. Zhou¹⁶², Y. Zhou¹⁵⁰, C.G. Zhu^{32d}, H. Zhu⁴¹, J. Zhu⁸⁶, Y. Zhu^{32b}, X. Zhuang⁹⁷, V. Zhuravlov⁹⁸, D. Zieminska⁵⁹, N.I. Zimin⁶³, R. Zimmermann²⁰, S. Zimmermann²⁰, S. Zimmermann⁴⁷, M. Ziolkowski¹⁴⁰, R. Zitoun⁴, L. Živković³⁴, V.V. Zmouchko^{127,*}, G. Zobernig¹⁷², A. Zoccoli^{19a,19b}, M. zur Nedden¹⁵, V. Zutshi¹⁰⁵, L. Zwalinski²⁹.

¹ Physics Department, SUNY Albany, Albany NY, United States of America

² Department of Physics, University of Alberta, Edmonton AB, Canada

³ (a) Department of Physics, Ankara University, Ankara; (b) Department of Physics, Dumlupinar University, Kutahya;

(c) Department of Physics, Gazi University, Ankara; (d) Division of Physics, TOBB University of Economics and Technology, Ankara; (e) Turkish Atomic Energy Authority, Ankara, Turkey

⁴ LAPP, CNRS/IN2P3 and Université de Savoie, Annecy-le-Vieux, France

⁵ High Energy Physics Division, Argonne National Laboratory, Argonne IL, United States of America

⁶ Department of Physics, University of Arizona, Tucson AZ, United States of America

⁷ Department of Physics, The University of Texas at Arlington, Arlington TX, United States of America

⁸ Physics Department, University of Athens, Athens, Greece

⁹ Physics Department, National Technical University of Athens, Zografou, Greece

¹⁰ Institute of Physics, Azerbaijan Academy of Sciences, Baku, Azerbaijan

¹¹ Institut de Física d'Altes Energies and Departament de Física de la Universitat Autònoma de Barcelona and ICREA, Barcelona, Spain

¹² (a) Institute of Physics, University of Belgrade, Belgrade; (b) Vinca Institute of Nuclear Sciences, University of Belgrade, Belgrade, Serbia

¹³ Department for Physics and Technology, University of Bergen, Bergen, Norway

¹⁴ Physics Division, Lawrence Berkeley National Laboratory and University of California, Berkeley CA, United States of America

¹⁵ Department of Physics, Humboldt University, Berlin, Germany

¹⁶ Albert Einstein Center for Fundamental Physics and Laboratory for High Energy Physics, University of Bern, Bern, Switzerland

¹⁷ School of Physics and Astronomy, University of Birmingham, Birmingham, United Kingdom

¹⁸ (a) Department of Physics, Bogazici University, Istanbul; (b) Division of Physics, Dogus University, Istanbul; (c) Department of Physics Engineering, Gaziantep University, Gaziantep; (d) Department of Physics, Istanbul Technical University, Istanbul, Turkey

¹⁹ (a) INFN Sezione di Bologna; (b) Dipartimento di Fisica, Università di Bologna, Bologna, Italy

²⁰ Physikalisches Institut, University of Bonn, Bonn, Germany

²¹ Department of Physics, Boston University, Boston MA, United States of America

²² Department of Physics, Brandeis University, Waltham MA, United States of America

²³ (a) Universidade Federal do Rio De Janeiro COPPE/EE/IF, Rio de Janeiro; (b) Federal University of Juiz de Fora (UFJF), Juiz de Fora; (c) Federal University of Sao Joao del Rei (UFSJ), Sao Joao del Rei; (d) Instituto de Física, Universidade de Sao Paulo, Sao Paulo, Brazil

²⁴ Physics Department, Brookhaven National Laboratory, Upton NY, United States of America

²⁵ (a) National Institute of Physics and Nuclear Engineering, Bucharest; (b) University Politehnica Bucharest, Bucharest; (c) West University in Timisoara, Timisoara, Romania

²⁶ Departamento de Física, Universidad de Buenos Aires, Buenos Aires, Argentina

- 27 Cavendish Laboratory, University of Cambridge, Cambridge, United Kingdom
- 28 Department of Physics, Carleton University, Ottawa ON, Canada
- 29 CERN, Geneva, Switzerland
- 30 Enrico Fermi Institute, University of Chicago, Chicago IL, United States of America
- 31 ^(a)Departamento de Física, Pontificia Universidad Católica de Chile, Santiago; ^(b)Departamento de Física, Universidad Técnica Federico Santa María, Valparaíso, Chile
- 32 ^(a)Institute of High Energy Physics, Chinese Academy of Sciences, Beijing; ^(b)Department of Modern Physics, University of Science and Technology of China, Anhui; ^(c)Department of Physics, Nanjing University, Jiangsu; ^(d)School of Physics, Shandong University, Shandong, China
- 33 Laboratoire de Physique Corpusculaire, Clermont Université and Université Blaise Pascal and CNRS/IN2P3, Aubiere Cedex, France
- 34 Nevis Laboratory, Columbia University, Irvington NY, United States of America
- 35 Niels Bohr Institute, University of Copenhagen, Kobenhavn, Denmark
- 36 ^(a)INFN Gruppo Collegato di Cosenza; ^(b)Dipartimento di Fisica, Università della Calabria, Arcavata di Rende, Italy
- 37 AGH University of Science and Technology, Faculty of Physics and Applied Computer Science, Krakow, Poland
- 38 The Henryk Niewodniczanski Institute of Nuclear Physics, Polish Academy of Sciences, Krakow, Poland
- 39 Physics Department, Southern Methodist University, Dallas TX, United States of America
- 40 Physics Department, University of Texas at Dallas, Richardson TX, United States of America
- 41 DESY, Hamburg and Zeuthen, Germany
- 42 Institut für Experimentelle Physik IV, Technische Universität Dortmund, Dortmund, Germany
- 43 Institut für Kern- und Teilchenphysik, Technical University Dresden, Dresden, Germany
- 44 Department of Physics, Duke University, Durham NC, United States of America
- 45 SUPA - School of Physics and Astronomy, University of Edinburgh, Edinburgh, United Kingdom
- 46 INFN Laboratori Nazionali di Frascati, Frascati, Italy
- 47 Fakultät für Mathematik und Physik, Albert-Ludwigs-Universität, Freiburg, Germany
- 48 Section de Physique, Université de Genève, Geneva, Switzerland
- 49 ^(a)INFN Sezione di Genova; ^(b)Dipartimento di Fisica, Università di Genova, Genova, Italy
- 50 ^(a)E. Andronikashvili Institute of Physics, Tbilisi State University, Tbilisi; ^(b)High Energy Physics Institute, Tbilisi State University, Tbilisi, Georgia
- 51 II Physikalisches Institut, Justus-Liebig-Universität Giessen, Giessen, Germany
- 52 SUPA - School of Physics and Astronomy, University of Glasgow, Glasgow, United Kingdom
- 53 II Physikalisches Institut, Georg-August-Universität, Göttingen, Germany
- 54 Laboratoire de Physique Subatomique et de Cosmologie, Université Joseph Fourier and CNRS/IN2P3 and Institut National Polytechnique de Grenoble, Grenoble, France
- 55 Department of Physics, Hampton University, Hampton VA, United States of America
- 56 Laboratory for Particle Physics and Cosmology, Harvard University, Cambridge MA, United States of America
- 57 ^(a)Kirchhoff-Institut für Physik, Ruprecht-Karls-Universität Heidelberg, Heidelberg; ^(b)Physikalisches Institut, Ruprecht-Karls-Universität Heidelberg, Heidelberg; ^(c)ZITI Institut für technische Informatik, Ruprecht-Karls-Universität Heidelberg, Mannheim, Germany
- 58 Faculty of Applied Information Science, Hiroshima Institute of Technology, Hiroshima, Japan
- 59 Department of Physics, Indiana University, Bloomington IN, United States of America
- 60 Institut für Astro- und Teilchenphysik, Leopold-Franzens-Universität, Innsbruck, Austria
- 61 University of Iowa, Iowa City IA, United States of America
- 62 Department of Physics and Astronomy, Iowa State University, Ames IA, United States of America
- 63 Joint Institute for Nuclear Research, JINR Dubna, Dubna, Russia
- 64 KEK, High Energy Accelerator Research Organization, Tsukuba, Japan
- 65 Graduate School of Science, Kobe University, Kobe, Japan
- 66 Faculty of Science, Kyoto University, Kyoto, Japan
- 67 Kyoto University of Education, Kyoto, Japan
- 68 Department of Physics, Kyushu University, Fukuoka, Japan
- 69 Instituto de Física La Plata, Universidad Nacional de La Plata and CONICET, La Plata, Argentina
- 70 Physics Department, Lancaster University, Lancaster, United Kingdom
- 71 ^(a)INFN Sezione di Lecce; ^(b)Dipartimento di Matematica e Fisica, Università del Salento, Lecce, Italy
- 72 Oliver Lodge Laboratory, University of Liverpool, Liverpool, United Kingdom
- 73 Department of Physics, Jožef Stefan Institute and University of Ljubljana, Ljubljana, Slovenia
- 74 School of Physics and Astronomy, Queen Mary University of London, London, United Kingdom
- 75 Department of Physics, Royal Holloway University of London, Surrey, United Kingdom
- 76 Department of Physics and Astronomy, University College London, London, United Kingdom

- 77 Laboratoire de Physique Nucléaire et de Hautes Energies, UPMC and Université Paris-Diderot and CNRS/IN2P3, Paris, France
- 78 Fysiska institutionen, Lunds universitet, Lund, Sweden
- 79 Departamento de Física Teórica C-15, Universidad Autónoma de Madrid, Madrid, Spain
- 80 Institut für Physik, Universität Mainz, Mainz, Germany
- 81 School of Physics and Astronomy, University of Manchester, Manchester, United Kingdom
- 82 CPPM, Aix-Marseille Université and CNRS/IN2P3, Marseille, France
- 83 Department of Physics, University of Massachusetts, Amherst MA, United States of America
- 84 Department of Physics, McGill University, Montreal QC, Canada
- 85 School of Physics, University of Melbourne, Victoria, Australia
- 86 Department of Physics, The University of Michigan, Ann Arbor MI, United States of America
- 87 Department of Physics and Astronomy, Michigan State University, East Lansing MI, United States of America
- 88 ^(a)INFN Sezione di Milano; ^(b)Dipartimento di Fisica, Università di Milano, Milano, Italy
- 89 B.I. Stepanov Institute of Physics, National Academy of Sciences of Belarus, Minsk, Republic of Belarus
- 90 National Scientific and Educational Centre for Particle and High Energy Physics, Minsk, Republic of Belarus
- 91 Department of Physics, Massachusetts Institute of Technology, Cambridge MA, United States of America
- 92 Group of Particle Physics, University of Montreal, Montreal QC, Canada
- 93 P.N. Lebedev Institute of Physics, Academy of Sciences, Moscow, Russia
- 94 Institute for Theoretical and Experimental Physics (ITEP), Moscow, Russia
- 95 Moscow Engineering and Physics Institute (MEPhI), Moscow, Russia
- 96 Skobeltsyn Institute of Nuclear Physics, Lomonosov Moscow State University, Moscow, Russia
- 97 Fakultät für Physik, Ludwig-Maximilians-Universität München, München, Germany
- 98 Max-Planck-Institut für Physik (Werner-Heisenberg-Institut), München, Germany
- 99 Nagasaki Institute of Applied Science, Nagasaki, Japan
- 100 Graduate School of Science and Kobayashi-Maskawa Institute, Nagoya University, Nagoya, Japan
- 101 ^(a)INFN Sezione di Napoli; ^(b)Dipartimento di Scienze Fisiche, Università di Napoli, Napoli, Italy
- 102 Department of Physics and Astronomy, University of New Mexico, Albuquerque NM, United States of America
- 103 Institute for Mathematics, Astrophysics and Particle Physics, Radboud University Nijmegen/Nikhef, Nijmegen, Netherlands
- 104 Nikhef National Institute for Subatomic Physics and University of Amsterdam, Amsterdam, Netherlands
- 105 Department of Physics, Northern Illinois University, DeKalb IL, United States of America
- 106 Budker Institute of Nuclear Physics, SB RAS, Novosibirsk, Russia
- 107 Department of Physics, New York University, New York NY, United States of America
- 108 Ohio State University, Columbus OH, United States of America
- 109 Faculty of Science, Okayama University, Okayama, Japan
- 110 Homer L. Dodge Department of Physics and Astronomy, University of Oklahoma, Norman OK, United States of America
- 111 Department of Physics, Oklahoma State University, Stillwater OK, United States of America
- 112 Palacký University, RCPTM, Olomouc, Czech Republic
- 113 Center for High Energy Physics, University of Oregon, Eugene OR, United States of America
- 114 LAL, Université Paris-Sud and CNRS/IN2P3, Orsay, France
- 115 Graduate School of Science, Osaka University, Osaka, Japan
- 116 Department of Physics, University of Oslo, Oslo, Norway
- 117 Department of Physics, Oxford University, Oxford, United Kingdom
- 118 ^(a)INFN Sezione di Pavia; ^(b)Dipartimento di Fisica, Università di Pavia, Pavia, Italy
- 119 Department of Physics, University of Pennsylvania, Philadelphia PA, United States of America
- 120 Petersburg Nuclear Physics Institute, Gatchina, Russia
- 121 ^(a)INFN Sezione di Pisa; ^(b)Dipartimento di Fisica E. Fermi, Università di Pisa, Pisa, Italy
- 122 Department of Physics and Astronomy, University of Pittsburgh, Pittsburgh PA, United States of America
- 123 ^(a)Laboratório de Instrumentação e Física Experimental de Partículas - LIP, Lisboa, Portugal; ^(b)Departamento de Física Teórica y del Cosmos and CAFPE, Universidad de Granada, Granada, Spain
- 124 Institute of Physics, Academy of Sciences of the Czech Republic, Praha, Czech Republic
- 125 Faculty of Mathematics and Physics, Charles University in Prague, Praha, Czech Republic
- 126 Czech Technical University in Prague, Praha, Czech Republic
- 127 State Research Center Institute for High Energy Physics, Protvino, Russia
- 128 Particle Physics Department, Rutherford Appleton Laboratory, Didcot, United Kingdom
- 129 Physics Department, University of Regina, Regina SK, Canada
- 130 Ritsumeikan University, Kusatsu, Shiga, Japan
- 131 ^(a)INFN Sezione di Roma I; ^(b)Dipartimento di Fisica, Università La Sapienza, Roma, Italy
- 132 ^(a)INFN Sezione di Roma Tor Vergata; ^(b)Dipartimento di Fisica, Università di Roma Tor Vergata, Roma, Italy
- 133 ^(a)INFN Sezione di Roma Tre; ^(b)Dipartimento di Fisica, Università Roma Tre, Roma, Italy

- 134 ^(a) Faculté des Sciences Ain Chock, Réseau Universitaire de Physique des Hautes Energies - Université Hassan II, Casablanca; ^(b) Centre National de l'Énergie des Sciences Techniques Nucleaires, Rabat; ^(c) Faculté des Sciences Semlalia, Université Cadi Ayyad, LPHEA-Marrakech; ^(d) Faculté des Sciences, Université Mohamed Premier and LTPM, Oujda; ^(e) Faculté des sciences, Université Mohammed V-Agdal, Rabat, Morocco
- 135 DSM/IRFU (Institut de Recherches sur les Lois Fondamentales de l'Univers), CEA Saclay (Commissariat à l'Énergie Atomique), Gif-sur-Yvette, France
- 136 Santa Cruz Institute for Particle Physics, University of California Santa Cruz, Santa Cruz CA, United States of America
- 137 Department of Physics, University of Washington, Seattle WA, United States of America
- 138 Department of Physics and Astronomy, University of Sheffield, Sheffield, United Kingdom
- 139 Department of Physics, Shinshu University, Nagano, Japan
- 140 Fachbereich Physik, Universität Siegen, Siegen, Germany
- 141 Department of Physics, Simon Fraser University, Burnaby BC, Canada
- 142 SLAC National Accelerator Laboratory, Stanford CA, United States of America
- 143 ^(a) Faculty of Mathematics, Physics & Informatics, Comenius University, Bratislava; ^(b) Department of Subnuclear Physics, Institute of Experimental Physics of the Slovak Academy of Sciences, Kosice, Slovak Republic
- 144 ^(a) Department of Physics, University of Johannesburg, Johannesburg; ^(b) School of Physics, University of the Witwatersrand, Johannesburg, South Africa
- 145 ^(a) Department of Physics, Stockholm University; ^(b) The Oskar Klein Centre, Stockholm, Sweden
- 146 Physics Department, Royal Institute of Technology, Stockholm, Sweden
- 147 Departments of Physics & Astronomy and Chemistry, Stony Brook University, Stony Brook NY, United States of America
- 148 Department of Physics and Astronomy, University of Sussex, Brighton, United Kingdom
- 149 School of Physics, University of Sydney, Sydney, Australia
- 150 Institute of Physics, Academia Sinica, Taipei, Taiwan
- 151 Department of Physics, Technion: Israel Institute of Technology, Haifa, Israel
- 152 Raymond and Beverly Sackler School of Physics and Astronomy, Tel Aviv University, Tel Aviv, Israel
- 153 Department of Physics, Aristotle University of Thessaloniki, Thessaloniki, Greece
- 154 International Center for Elementary Particle Physics and Department of Physics, The University of Tokyo, Tokyo, Japan
- 155 Graduate School of Science and Technology, Tokyo Metropolitan University, Tokyo, Japan
- 156 Department of Physics, Tokyo Institute of Technology, Tokyo, Japan
- 157 Department of Physics, University of Toronto, Toronto ON, Canada
- 158 ^(a) TRIUMF, Vancouver BC; ^(b) Department of Physics and Astronomy, York University, Toronto ON, Canada
- 159 Institute of Pure and Applied Sciences, University of Tsukuba, 1-1-1 Tennodai, Tsukuba, Ibaraki 305-8571, Japan
- 160 Science and Technology Center, Tufts University, Medford MA, United States of America
- 161 Centro de Investigaciones, Universidad Antonio Narino, Bogota, Colombia
- 162 Department of Physics and Astronomy, University of California Irvine, Irvine CA, United States of America
- 163 ^(a) INFN Gruppo Collegato di Udine; ^(b) ICTP, Trieste; ^(c) Dipartimento di Chimica, Fisica e Ambiente, Università di Udine, Udine, Italy
- 164 Department of Physics, University of Illinois, Urbana IL, United States of America
- 165 Department of Physics and Astronomy, University of Uppsala, Uppsala, Sweden
- 166 Instituto de Física Corpuscular (IFIC) and Departamento de Física Atómica, Molecular y Nuclear and Departamento de Ingeniería Electrónica and Instituto de Microelectrónica de Barcelona (IMB-CNM), University of Valencia and CSIC, Valencia, Spain
- 167 Department of Physics, University of British Columbia, Vancouver BC, Canada
- 168 Department of Physics and Astronomy, University of Victoria, Victoria BC, Canada
- 169 Department of Physics, University of Warwick, Coventry, United Kingdom
- 170 Waseda University, Tokyo, Japan
- 171 Department of Particle Physics, The Weizmann Institute of Science, Rehovot, Israel
- 172 Department of Physics, University of Wisconsin, Madison WI, United States of America
- 173 Fakultät für Physik und Astronomie, Julius-Maximilians-Universität, Würzburg, Germany
- 174 Fachbereich C Physik, Bergische Universität Wuppertal, Wuppertal, Germany
- 175 Department of Physics, Yale University, New Haven CT, United States of America
- 176 Yerevan Physics Institute, Yerevan, Armenia
- 177 Domaine scientifique de la Doua, Centre de Calcul CNRS/IN2P3, Villeurbanne Cedex, France
- ^a Also at Laboratorio de Instrumentacao e Fisica Experimental de Particulas - LIP, Lisboa, Portugal
- ^b Also at Faculdade de Ciencias and CFNUL, Universidade de Lisboa, Lisboa, Portugal
- ^c Also at Particle Physics Department, Rutherford Appleton Laboratory, Didcot, United Kingdom
- ^d Also at TRIUMF, Vancouver BC, Canada
- ^e Also at Department of Physics, California State University, Fresno CA, United States of America
- ^f Also at Novosibirsk State University, Novosibirsk, Russia

- ^g Also at Fermilab, Batavia IL, United States of America
^h Also at Department of Physics, University of Coimbra, Coimbra, Portugal
ⁱ Also at Department of Physics, UASLP, San Luis Potosi, Mexico
^j Also at Università di Napoli Parthenope, Napoli, Italy
^k Also at Institute of Particle Physics (IPP), Canada
^l Also at Department of Physics, Middle East Technical University, Ankara, Turkey
^m Also at Louisiana Tech University, Ruston LA, United States of America
ⁿ Also at Dep Física and CEFITEC of Faculdade de Ciências e Tecnologia, Universidade Nova de Lisboa, Caparica, Portugal
^o Also at Department of Physics and Astronomy, University College London, London, United Kingdom
^p Also at Group of Particle Physics, University of Montreal, Montreal QC, Canada
^q Also at Department of Physics, University of Cape Town, Cape Town, South Africa
^r Also at Institute of Physics, Azerbaijan Academy of Sciences, Baku, Azerbaijan
^s Also at Institut für Experimentalphysik, Universität Hamburg, Hamburg, Germany
^t Also at Manhattan College, New York NY, United States of America
^u Also at School of Physics, Shandong University, Shandong, China
^v Also at CPPM, Aix-Marseille Université and CNRS/IN2P3, Marseille, France
^w Also at School of Physics and Engineering, Sun Yat-sen University, Guanzhou, China
^x Also at Academia Sinica Grid Computing, Institute of Physics, Academia Sinica, Taipei, Taiwan
^y Also at Dipartimento di Fisica, Università La Sapienza, Roma, Italy
^z Also at DSM/IRFU (Institut de Recherches sur les Lois Fondamentales de l'Univers), CEA Saclay (Commissariat à l'Energie Atomique), Gif-sur-Yvette, France
^{aa} Also at Section de Physique, Université de Genève, Geneva, Switzerland
^{ab} Also at Departamento de Física, Universidade de Minho, Braga, Portugal
^{ac} Also at Department of Physics and Astronomy, University of South Carolina, Columbia SC, United States of America
^{ad} Also at Institute for Particle and Nuclear Physics, Wigner Research Centre for Physics, Budapest, Hungary
^{ae} Also at California Institute of Technology, Pasadena CA, United States of America
^{af} Also at Institute of Physics, Jagiellonian University, Krakow, Poland
^{ag} Also at LAL, Université Paris-Sud and CNRS/IN2P3, Orsay, France
^{ah} Also at Nevis Laboratory, Columbia University, Irvington NY, United States of America
^{ai} Also at Department of Physics and Astronomy, University of Sheffield, Sheffield, United Kingdom
^{aj} Also at Department of Physics, Oxford University, Oxford, United Kingdom
^{ak} Also at Institute of Physics, Academia Sinica, Taipei, Taiwan
^{al} Also at Department of Physics, The University of Michigan, Ann Arbor MI, United States of America
* Deceased